Executive Summary

CAER

A mathematical model has been developed to describe the product distribution of Fischer-Tropsch synthesis, based on the recognition that the termination path to olefin is reversible. The observed product distribution at the reactor outlet consists of the contribution from intrinsic chain propagation on catalyst surface and the effect of olefin reincorporation. The 2-alpha distribution can be attributed to the effect of vapor liquid separation of hydrocarbon products. The reaction product does not follow ASF single alpha distribution any more even on catalyst surface. A tight fit between model prediction and experimental data has been demonstrated. Also, the deviation point of product distribution is precisely predicted to be within carbon number 8-14 under typical FT conditions.

In order to understand how branched alkenes and alkanes are formed, it is necessary to quantitatively measure each isomer of each carbon number. Since some of the branched alkanes overlap the branched alkenes and vice-versa, it becomes necessary to use indirect means to measure the amount of each isomer. In this study, the FT products were hydrogenated and brominated, and an accurate amount of each branch alkane was obtained.

The mole percent of branched alkanes in Fe catalyzed FT products varies from run to run. However, within the run, different carbon number compounds have about the same mole percent of branched alkanes. This is also true for Co catalyzed FT reactions. The major difference between Fe and Co catalyzed FT reaction in terms of mole percent of branched alkanes is that Co catalyzed FT synthesis reactions produce only 1-4% of branched alkanes, whereas the Fe catalyzed FT reactions can produce as high as 20% (and probably more) of branched alkanes.

The effect of the addition of water during Fischer-Tropsch synthesis was studied using a ruthenium promoted Co/TiO_2 catalyst. At low conversions (space velocities greater than 4 NL^{-1} $cat.hr^{-1}$) the addition of water to the feed did not have a significant effect on the synthesis gas conversion. However, at high conversion levels (low space velocities), the addition of water decreased the synthesis gas conversion. At the high space velocities, the hydrocarbon production rate was not changed with the addition of water. At low space velocities, the addition of water resulted in a decrease in the production rate. For all the space velocities studied, the methane selectivities were not significantly changed with the addition of water. The addition of water increased the CO_2 selectivity by approximately two times that of the system with no water addition. This showed that the addition of water enhanced the water-gas shift reaction.

Four runs were made using high-alpha catalysts ($\alpha_2 > 0.9$) to evaluate four special filters for their ability to internally separate the wax from the catalyst slurry. Each filter was one inch in diameter but had different filter surface areas (1.57, 3.14 and 4.71 cm^3), pore sizes (2μ and 18μ) and filter lengths (0.5, 1.0 and 1.5 inches). All four filters performed well for the 1000 hours of the experiments. Each filter allowed over 100g of wax (total) to be removed during the run. For two of the filters, the Fe content of the wax removed was determined. Approximately 8 - 9.6% of Fe charged to the reactor was lost during the 1000 hours of the two runs.

UC/B

In this reporting period, we have started the preparation of a new series of catalysts based on Fe-Zn oxide precursors containing various concentrations of Ru and K promoters. The structure, reduction and carburization behavior, and catalytic properties of Fischer-Tropsch synthesis (FTS) catalysts based on K- and Ru-promoted Fe-Zn oxides have been studied using temperature-programmed reduction and carburization in H_2 and CO and transient reaction

methods in synthesis gas at FTS conditions. The results showed that Fe-Zn oxides reduce at lower temperatures than pure Fe_2O_3 because of the presence of $ZnFe_2O_4$ which acts as nuclei for the conversion from Fe_2O_3 to Fe_3O_4. Ru addition increases Fe oxide reduction by providing H_2 dissociation sites and increases carburization rates by dissociating CO. The addition of K slightly inhibits H_2 and CO reduction but increases carburization rates by assisting CO dissociation. Isothermal transients studies on Fe-Zn-Ru-K oxides at FTS conditions showed that Ru increases FTS rates by increasing reduction and carburization rates and by providing more active sites. Combined with K, Ru-promoted Fe-Zn oxides showed slightly higher initial CH_4 formation rates and reached steady state values (~0.03 mmol/g-atom Fe s) earlier than the sample without K. We have also continued our X-ray absorption studies at the Stanford Synchrotron Radiation Laboratory (SSRL) with emphasis on measuring the spectra at FTS conditions (543 K, 5 atm) and with the CO_2 addition in order to simulate high conversion conditions and to explore any phase changes in these catalysts. The results showed that the stability of Fe oxide or carbide phases is determined by the CO_2/CO ratio in reaction stream. The oxidation of initially formed Fe carbides to Fe_3O_4 requires a large CO_2/CO ratio (>13.0) at the conditions investigated (543 K and 1 atm).

Fischer-Tropsch synthesis reactions were carried out on Fe-Zn-Ru catalyst samples (Zn/Fe=0.1, Ru/M=0.01) at three different conditions (220 ºC, 30 atm; 235 ºC, 21.4 atm; and 270ºC, 5 atm). The reaction results were compared with those for Fe-Zn-Cu catalyst studied previously at similar CO space velocities. CO conversion rates were significantly higher on Fe-Zn-Ru (3.1 mol/h.g-at Fe compared to 1.2 mol/h.g-at Fe on Fe-Zn-Cu at a CO space velocity of 5.3 NL/hr.g-Fe and 220 ºC). CO_2 selectivities were higher on the Ru-promoted catalyst (17% on Fe-Zn-Ru compared to 8% on Fe-Zn-Cu at 20% CO conversion and 235 ºC). CH_4 selectivities

were lower on Fe-Zn-Ru (7% on Fe-Zn-Ru compared to 10% on Fe-Zn-Cu at 20% CO conversion and 235 ºC). The C_{5+} hydrocarbon selectivity was higher over Fe-Zn-Ru (71% on Fe-Zn-Ru compared to 61% on Fe-Zn-Cu at 20% CO conversion and 235 ºC).

FTS reaction studies on Fe-Zn-Ru (Zn/Fe=0.1, Ru/M=0.01) and Fe-Zn-Ru-K (Zn/Fe=0.1, Ru/M=0.01, K/M=0.02) catalysts showed that the addition of K had different effects at the three reaction conditions. At the lower temperatures, *i.e.*, 220 ºC and 235 ºC, the addition of K increased CO conversion and hydrocarbon synthesis rates. At 270 ºC, the presence of K caused a decrease in the CO conversion and hydrocarbon synthesis rates. The CO_2 selectivities increased with K-addition at all three temperatures (*e.g.* ~18% to ~31% at 30% CO conversion and 235 ºC) similar to that observed for the Fe-Zn-Cu system. In addition, CH_4 selectivities decreased (from ~7% to ~3%) and the C_{5+} selectivities increased (from ~71% to ~86%) at 235 ºC with the addition of K to the Fe-Zn-Ru catalyst, at all conditions.

During this reporting period, a non-linear multivariate regression program was completed in Matlab and a couple of the mechanisms proposed earlier to explain FTS reaction kinetics over Co/SiO_2 catalysts were tested for conformance to the reaction data. From this regression program, the various kinetic parameters based on the rate constants of the elementary steps were obtained. A comparison of the measured reaction rates with the rates predicted by the two mechanisms show that in both cases, the predicted rate was within 95% of the measured values. This appears to indicate that both the proposed mechanisms are consistent with the reaction kinetics on Co/SiO_2 catalysts.

As part of our efforts to eliminate discrepancies in hydrocarbon selectivities associated with the Co/SiO_2 system, the GC response factors were recalibrated with a standard gas mixture. There were significant differences in the CH_4 and CO response factors, which in turn resulted in a

minimization of the deviation in the hydrocarbon selectivity numbers that were reported previously. Still, there were some small differences in the hydrocarbon selectivities and α-olefin/*n*-paraffin ratios, which could be due to hydrogenation on the walls of the reactor.

Task 1. Iron Catalyst Preparation

The objective of this task is to produce robust intermediate- and high-α catalysts.

No scheduled activity to report.

Task 2. Catalyst Testing

The objective of this task is to obtain catalyst performance on the catalysts prepared in Task 1.

A. The Formation of Branched Hydrocarbons in the Fe and Co Catalyzed FT Reactions

Introduction

To fully understand the mechanism for the FT reactions, it is important to understand how branched alkanes and alkenes being formed. If they are the products of the secondary reactions, the question to be answered is how and under what conditions that they are produced. On the other hand, if they are the primary products of the FT reactions, then it is necessary for any mechanistic scheme proposed for FT reactions to include the formation of branched alkenes and alkanes. In this study, we want to know how much branched hydrocarbon is formed under different conditions and different catalysts and try to understand which factor or factors plays the more important role in the formation of the branched products.

In order to understand how branched alkenes and alkanes being formed, it is necessary to quantitatively measure each isomers of each carbon number. Since some GC peaks of branched alkanes were buried in the branched alkene peaks and the vise versa, it is necessary to use indirect means to measure the amount of each isomer. In this study, the FT products were hydrogenated or brominated and an accurate amount of each branched alkane was obtained.

Experimental

1. Hydrogenation of FT Products

Six grams of FT products (oil and wax) and 0.5 g of Pt/C were placed in a jar. The reaction mixture was reduced under hydrogen pressure (30 psig) at room temperature with excellent stirring until no alkenes were found in the reaction mixture. Then the reaction mixture was filtered prior to GC and GC/MS analysis. The FT products hydrogenated are the following: for Fe catalyzed FT products: Bao20, Bao22, Bao26, Bao28 and Bao29; for Co catalyzed FT products: L366, L367 and L368 (Table 1).

2. Bromination of FT Products

To the FT oil (for some samples, oil and wax), 22.3% bromine in acetic acid was added drop by drop with vigorously stirring until the solution gave a permanent yellow to orange color. The oils brominated are: for Fe catalyzed FT products: Bao20, Bao22, Bao26, Bao28 and Bao29; for Co catalyzed FT products: L366, L367 and L368.

3. Analysis of FT Products

The FT oil and the samples after hydrogenation and bromination were analyzed by GC and GC/MS. The branched alkanes in each carbon number were identified by GC/MS, and quantitatively determined by GC/FID.

Results and Discussion

Five oil samples from Fe catalyzed FT reactions and 3 oil samples from Co catalyzed FT reactions were hydrogenated and brominated. The FT reaction conditions and the catalyst compositions were given in Tables 1 and 2.

All of the FT products in the runs reported in this report contain 1-alkene, alkane, 2-alkenes, alcohols as well as branched hydrocarbons. After hydrogenation, the alkenes were

converted to corresponding alkanes; after bromination, the alkenes were converted to corresponding dibromides.

Figure 1 is a partial chromatogram of the sample from Fe catalyzed FT reaction (Bao20). The top curve in this figure is for the FT products; the bottom figure is the sample after bromination and the middle chromatogram is for the sample after hydrogenation.

Figures 2 through 6 are the chromatograms of carbon 7, 8, 9, 10 and 11 of run Bao20, respectively. Again, the top in each figure is the FT products; the middle, after hydrogenation; and the bottom, after bromination (for the other 4 Fe catalyzed FT samples, the figures are similar and are not reproted). After hydrogenation, the branched alkenes were converted to the corresponding branched alkanes and normal alkenes were converted to normal the alkane. The mole percent of branched alkanes of each carbon number is defined as:

$$\%\ branched = \frac{branched\ alkanes}{branched\ alkanes + normal\ alkane} X\ 100 \qquad \textbf{(1)}$$

In the case of hydrogenated sample, the % branched alkanes represent the total branched hydrocarbons (branched alkenes plus branched alkanes). Since it is difficult to quantitatively measure the amount of branched alkanes in the original FT oil due to peak overlap, bromination of the FT oil is useful. The bromination of FT oil enable us to quantitatively measure the % branched alkanes from C_7 to C_{11} since the dibromide formed from these olefins elute following C_{11}. In this case, the % branched alkanes represents the total branched alkanes in the reaction product. The results are given in Tables 3-7 for Fe catalyzed FT reactions produced in runs Bao20, Bao22, Bao26, Bao28 and Bao29, respectively.

Figure 7 is the partial chromatogram of a sample from the Co catalyzed FT reaction (L366), and Figures 8 through 12 are the chromatograms of carbon numbers 7, 8, 9, 10 and 11 formed during run L366, respectively. The chromatograms of the other two Co catalyzed FT

runs (L367 and L368) are similar to Figures 7 through 12. As Figures 1 through 6, the top is the FT products; the middle, after hydrogenation; bottom, after bromination. The mole percent of branched alkanes are compiled in Table 8.

As can be seen from Tables 3 and 4, Runs Bao20 and Bao22 were conducted using the same catalyst and same reaction conditions except temperature. Bao20 was run at 230°C and Bao22 was run at 270°C. As the reaction temperature was increased, the amount of branched alkanes in most of the carbon numbers increased by more than 5%.

Runs Bao22 and Bao26 (data in Table 4 and Table 5) were conducted using the same catalyst at the same temperature but at different H_2:CO ratios and WHSV. When the H2:CO ratio increased from 0.67 to 1.70 and the WHSV increased from 10 to 40, the amount of branched alkanes (Bao26) decreased by 5-10% for all of the carbon numbers, with few exceptions.

In all of the five Fe catalyzed FT runs, it appears that the catalyst composition has a more significant impact on the formation of branched hydrocarbons than the reaction conditions, such as temperature, flow rate and H_2:CO ratio. The only difference between runs Bao26 (data in Table 5) and Bao28 (data in Table 6) is that the catalyst used in the run Bao28 differs slightly from that of Bao26 (1.4% and 4% K, respectively), and yet the amount of the branched alkanes increased more than 10% for most carbon numbers for the higher potassium containing catalyst.

Run Bao29 was conducted using pure Fe catalyst (100% Fe). The amount of branched alkanes (data in Table 7) is lower than runs Bao22 and Bao28. Since this run was also conducted at a higher H_2:CO ratio, lower temperature and lower WHSV, it is difficult to tell which factor played the major role.

The major difference between Fe catalyzed FT reactions and Co catalyzed FT reactions is the production of larger amounts of branched hydrocarbons with the catalyzed FT reaction. As can be seen from Tables 3 through 8, the Fe catalyzed FT reaction produced 10 to 25% of branched hydrocarbon (data after hydrogenation), whereas the Co catalyzed FT reaction produced only 1-4% of branched hydrocarbons (Table 8).

The reaction conditions of the three Co catalyzed FT reactions are different (see Table 2) and the catalyst compositions are also slightly different. Therefore, it is hard to tell which factor is more responsible for the formation of the branched hydrocarbons. Run L367 produced highest percentage of branched hydrocarbons (about 4%) among these three runs and this is probably due to the low WHSV.

The mole percent of branched alkanes after hydrogenation is the percentage of total branched hydrocarbons (branched alkenes and branched alkanes) in the total hydrocarbons. Designating the P_B as branched alkanes; O_B, branched alkenes; P_n, normal alkane; O_n, normal alkenes, then after hydrogenation, we have:

$$Mol\%\ (branched\ alkanes\ after\ hydrogenation) = \frac{P_B + O_B}{P_B + O_B + P_n + O_n} X\ 100 \qquad \textbf{(2)}$$

The mole percent of branched alkanes after FT reaction can be represented by the mole percent of branched alkanes after bromination as shown in eq. 3:

$$Mol\%(branched\ alkanes\ after\ bromination) = \frac{P_B}{P_B + P_n} X\ 100 \qquad \textbf{(3)}$$

If $O_n/P_n = O_B/P_B$, it can be proven that

Mol% (branched alkanes after [H]) = Mol% (branched alkanes after [Br]) **(4)**

However, if $O_n/P_n < O_B/P_B$, then

Mol% (branched alkanes after [H]) > Mol% (branched alkanes after [Br]) **(5)**

And if $O_n/P_n > O_B/P_B$, then

Mol% (branched alkanes after [H]) < Mol% (branched alkanes after [Br]) **(6)**

As seen in Figures 13 through 17 for in Fe catalyzed FT reactions, the mole percent of branched alkane after hydrogenation in all of these five runs is either higher than or close to that of the branched alkanes after bromination. This indicated that the ratio of O_n/P_n is less than or close to the ratio of O_B/P_B. These results suggest that during the formation of these FT products, the rate of hydrogenation of n-alkenes is close to or only slightly larger than that of branched alkenes. Similar results were obtained for Co catalyzed FT reactions (Figures 18 through 20).

The relative ratio of n-alkenes/n-alkane (O_n/P_n) can be measured accurately based on the GC. Because of the GC peak overlap, it is very difficult to measure accurately the ratio of branched-alkenes/branched alkanes (O_B/P_B). However, the ratio of O_B/P_B can be calculated based on the mole percent of the branched alkanes (after hydrogenation and after bromination) and the ratio of O_n/P_n.

Let

$$(P_B + O_B)/(P_B + O_B + P_n + O_n) = \alpha \quad \textbf{(7)}$$

where α is the mole percent of branched alkanes after hydrogenation, and

$$P_B/(P_B + P_n) = \beta \quad \textbf{(8)}$$

where β is the mole percent of branched alkanes after bromination. The ratio of n-alkenes/n-alkane is represented in eq. 9:

$$O_n/P_n = \gamma \quad \textbf{(9)}$$

Solving the eq. 7, 8 and 9, we have

$$O_B/P_B = \frac{\alpha(1-\beta)(1+\gamma)-\beta(1-\alpha)}{\beta(1-\alpha)} \quad \textbf{(10)}$$

Based on eq. 10, the ratio of O_B/P_B can be calculated. Also based on the eq. 10, it can be proven that if $\alpha = \beta$, then $O_B/P_B = O_n/P_n = \gamma$; if $\alpha > \beta$, then $O_B/P_B > O_n/P_n$; if $\alpha < \beta$, then $O_B/P_B < O_n/P_n$.

The representative results were given in Table 9 (for Fe catalyzed FT reactions) and Table 10 (for Co catalyzed FT reactions).

The mole percent of branched alkanes in Fe catalyzed FT products (Figure 21) varies from run to run. However, for any run, the different carbon number compounds have about same mole percent of branched alkanes. This is also true for Co catalyzed FT reactions (Figure 22). The major difference between Fe and Co catalyzed FT reaction in term of mole percent of branched alkanes is that Co catalyzed FT reactions only produce 1-4% of branched alkanes, whereas the Fe catalyzed FT reactions can produce as high as 20% (probably more) of branched alkanes.

Table 1

The Reaction Conditions and the Catalyst in the Fe Catalyzed FT Reactions

Run ID	Bao20	Bao22	Bao26	Bao28	Bao29
Catalyst	4.6% Si, 64.6% Fe, 2.0% Cu, 1.4% K	4.6% Si, 64.6% Fe, 2.0% Cu, 1.4% K	4.6% Si, 64.6% Fe, 2.0% Cu, 1.4% K	4.6% Si, 62.2% Fe, 2.0% Cu, 5% K	100% Fe
Temp. (^{o}C)	230	270	270	270	255
H_2 : CO	0.67	0.67	1.70	1.70	1.91
WHSV	10	10	40	40	3.0

Table 2

The Reaction Conditions and the Catalyst in the Co Catalyzed FT Reactions

Run ID	L366	L367	L368
Catalyst	10% Co/0.2% Ru/ TiO_2	15% Co/ 0.5% Ru/ SiO_2	15% Co/ 0.53% Pt/ Al_2O_3
temp. (^oC)	230	220	220
Pressure (psig)	350	300	275
H_2 : CO	2	2	2
WHSV	18.29	6.73	13.40

Table 3

The Mole Percent of Branched Alkanes in Fe Catalyzed FT Products (Run ID: Bao20)

	FT Products		After Hydrogenation		After Bromination	
Carbon #	# of isomers	Mol%	# of isomers	Mol%	# of isomers	Mol%
7	-	-	2	15.12	2	11.03
8	2	26.1	3	14.50	3	14.43
9	3	18.12	3	11.51	3	11.31
10	2	12.06	6	12.59	4	11.15
11	4	12.23	4	8.93	4	9.68
12	3	4.58	5	7.16		
13	3	7.43	5	11.61		

Table 4

The Mole Percent of Branched Alkanes in Fe Catalyzed Ft Products (Run ID: Bao22)

	FT Products		After Hydrogenation		After Bromination	
Carbon #	# of isomers	Mol%	# of isomers	Mol%	# of isomers	Mol%
7	2	8.82	2	16.05	2	5.10
8	3	17.67	3	19.71	3	15.92
9	3	16.60	5	19.01	3	15.32
10	4	12.69	5	19.06	4	17.27
11	4	11.89	5	20.00	4	17.27
12	4	18.94	5	15.47		
13	5	21.71	5	20.43		

Table 5

The Mole Percent of Branched Alkanes in Fe Catalyzed FT Products (Run ID: Bao26)

	FT Products		After Hydrogenation		After Bromination	
Carbon #	# of isomers	Mol%	# of isomers	Mol%	# of isomers	Mol%
7	2	9.81	2	9.03	2	10.44
8	3	15.67	3	8.89	3	11.25
9	3	9.62	3	10.05	3	9.42
10	4	9.44	5	10.39	4	9.02
11	4	9.57	4	9.37	4	5.72
12	3	6.14	4	8.35		
13	4	5.89	5	9.15		

Table 6

The Mole percent of Branched Alkanes in Fe Catalyzed FT Products (Run ID: Bao28)

	FT Products		After Hydrogenation		After Bromination	
Carbon #	# of isomers	Mol%	# of isomers	Mol%	# of isomers	Mol%
7	-	-	2	14.82	2	19.21
8	2	19.68	2	25.74	3	18.04
9	3	18.50	7	20.73	3	18.04
10	3	20.86	7	19.99	3	16.41
11	4	24.77	6	19.42	4	11.71

Table 7

The Mole Percent of Branched Alkanes in Fe Catalyzed FT Products (Run ID: Bao29)

	FT Products		After Hydrogenation		After Bromination	
Carbon #	# of isomers	Mol%	# of isomers	Mol%	# of isomers	Mol%
7	-	-	2	10.05	2	13.48
8	2	15.18	3	14.50	3	14.58
9	3	13.86	3	10.89	3	11.90
10	3	12.88	6	12.27	4	11.55
11	4	11.83	5	10.37	5	11.43
12	-	-	-	-	-	-
13	-	-	-	-	-	-

Table 8
The Mole percent of Branched Alkanes in Co Catalyzed FT Products

		FT Products		After Hydrogenation		After Bromination	
Carbon #	Run #	# of isomers	Mol%	# of isomers	Mol%	# of isomers	Mol%
7	L366	2	1.85	2	1.99	2	1.40
	L367	2	7.52	2	6.00	2	3.71
	L368	2	2.28	2	1.55	2	1.18
8	L366	2	2.33	2	2.45	3	1.67
	L367	3	4.69	3	4.15	3	4.05
	L368	3	2.26	3	1.57	3	1.35
9	L366	3	2.81	3	2.17	3	2.06
	L367	3	4.80	3	3.78	3	4.10
	L368	3	1.53	3	1.62	3	1.34
10	L366	3	2.19	3	2.39	3	2.08
	L367	4	4.34	4	4.05	4	4.29
	L368	3	1.51	3	1.61	3	1.37
11	L366	4	2.62	4	2.79	4	2.00
	L367	4	4.47	4	4.26	4	4.35
	L368	4	1.69	4	1.84	4	1.84
12	L366	4	1.87	5	3.02		
	L367	5	4.31	5	4.26		
	L368	4	1.60	4	1.73		
13	L366	5	3.10	5	3.34		
	L367	5	4.70	5	4.59		
	L368	5	1.84	5	1.96		
14	L366	5	3.45	5	3.72		
	L367	5	4.88	5	4.86		
	L368	-	-	-	-		

Table 9

The Relative Ratio of the Products in Fe Catalyzed FT reactions (Run ID: Bao22)

Carbon Number	branched- hydrocarbons/ total- hydrocarbons	branched-alkanes/ total alkanes	n-alkenes/ n-alkane	branched-alkenes/ branched alkanes
7	0.1605	0.051	2.3329	1.8574
8	0.1971	0.1592	2.0029	1.9647
9	0.1901	0.1532	1.6416	1.6063
10	0.1906	0.1727	1.4831	1.4688
11	0.2000	0.1727	1.2705	1.2516

Table 10

The Relative Ratio of the Products in Co Catalyzed FT reactions (Run ID: L367)

Carbon Number	branched- hydrocarbons/ total- hydrocarbons	branched-alkanes/ total alkanes	n-alkenes/ n-alkane	branched-alkenes/ branched alkanes
7	0.0600	0.0371	0.371	0.2018
8	0.0415	0.0405	0.2973	0.2871
9	0.0378	0.041	0.2390	0.2738
10	0.0405	0.0429	0.1973	0.2193
11	0.0426	0.0435	0.1645	0.1719

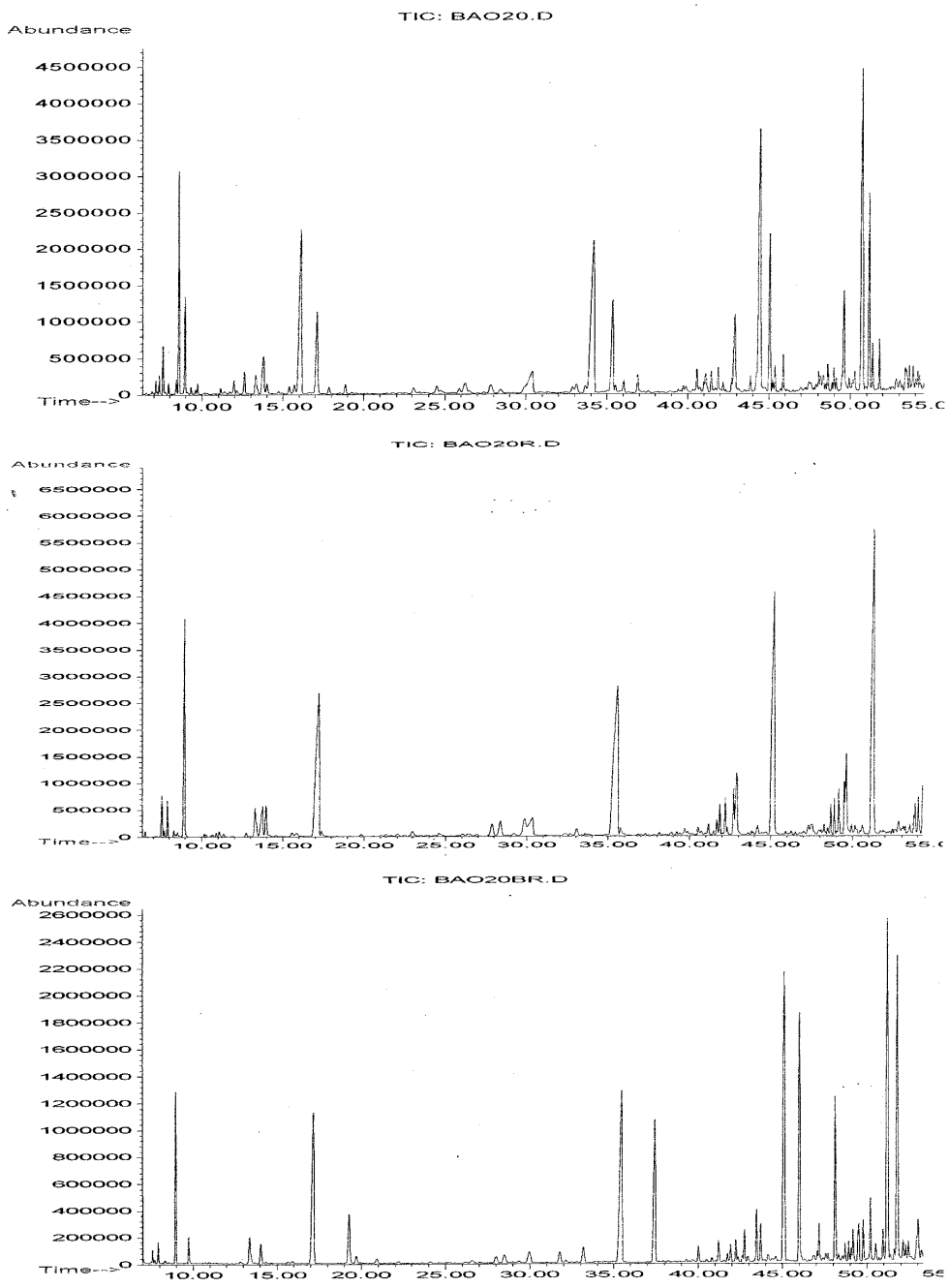

Figure 1. The Partial Chromatogram of the Oil Sample from Fe Catalyzed FT reaction (Run ID: Bao20) (Top: FT products; Middle: after hydrogenation; Bottom: after bromination).

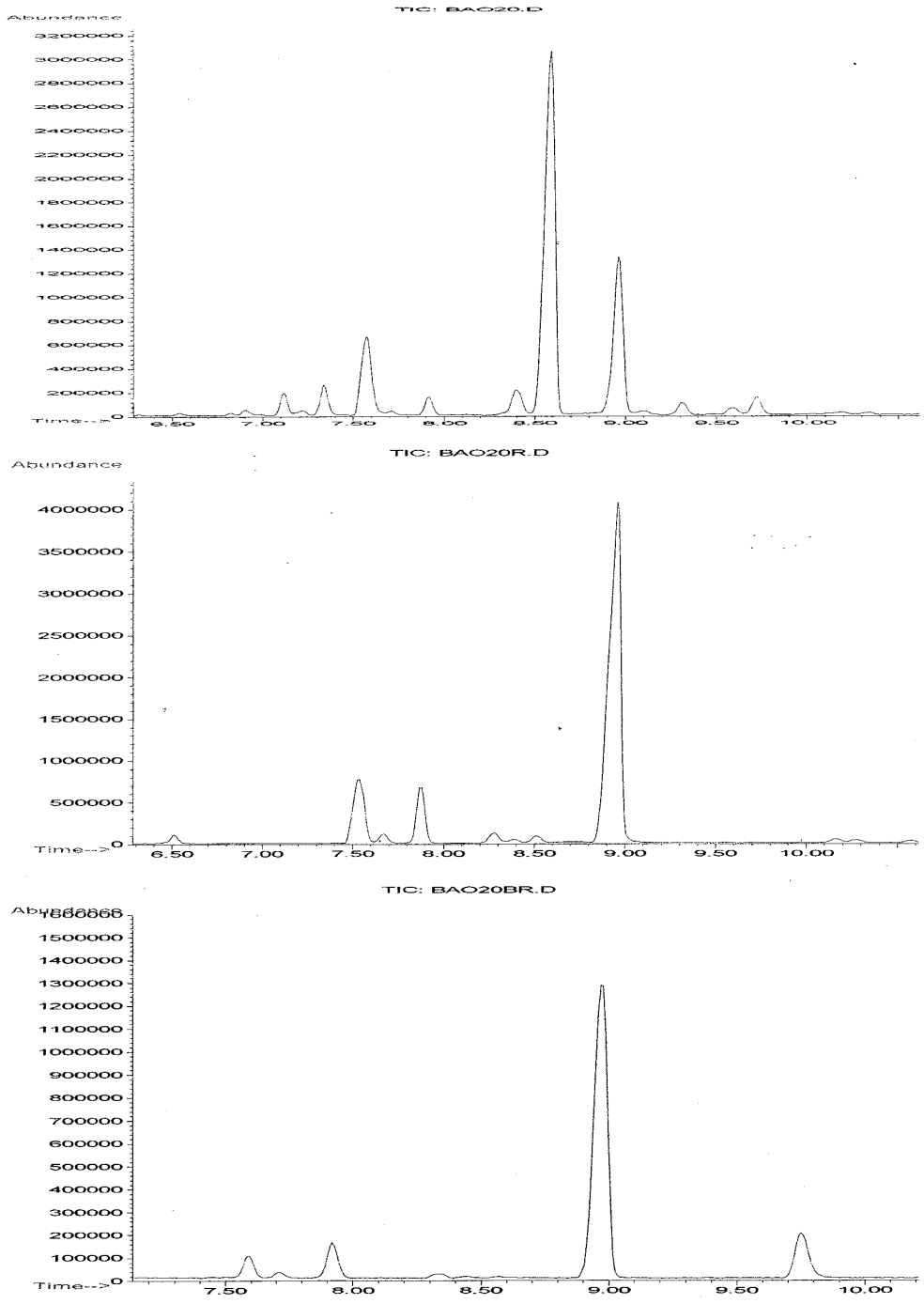

Figure 2. The Chromatogram of the Carbon-7 of the Run Bao20 (Top: FT products; Middle: after hydrogenation; Bottom: after bromination).

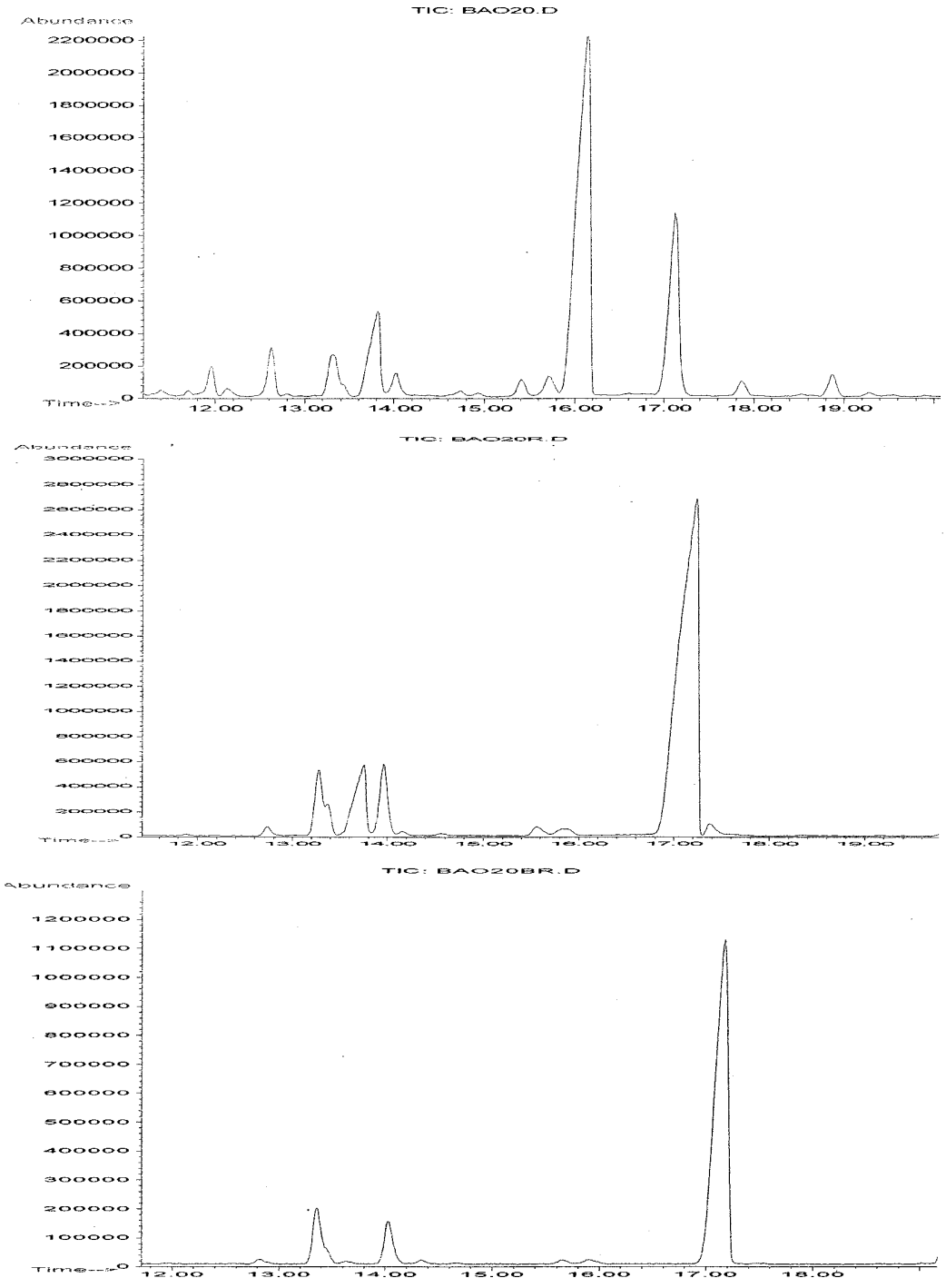

Figure 3. The Chromatogram of the Carbon-8 of the Run Bao20 (Top: FT products; Middle: after hydrogenation; Bottom: after bromination).

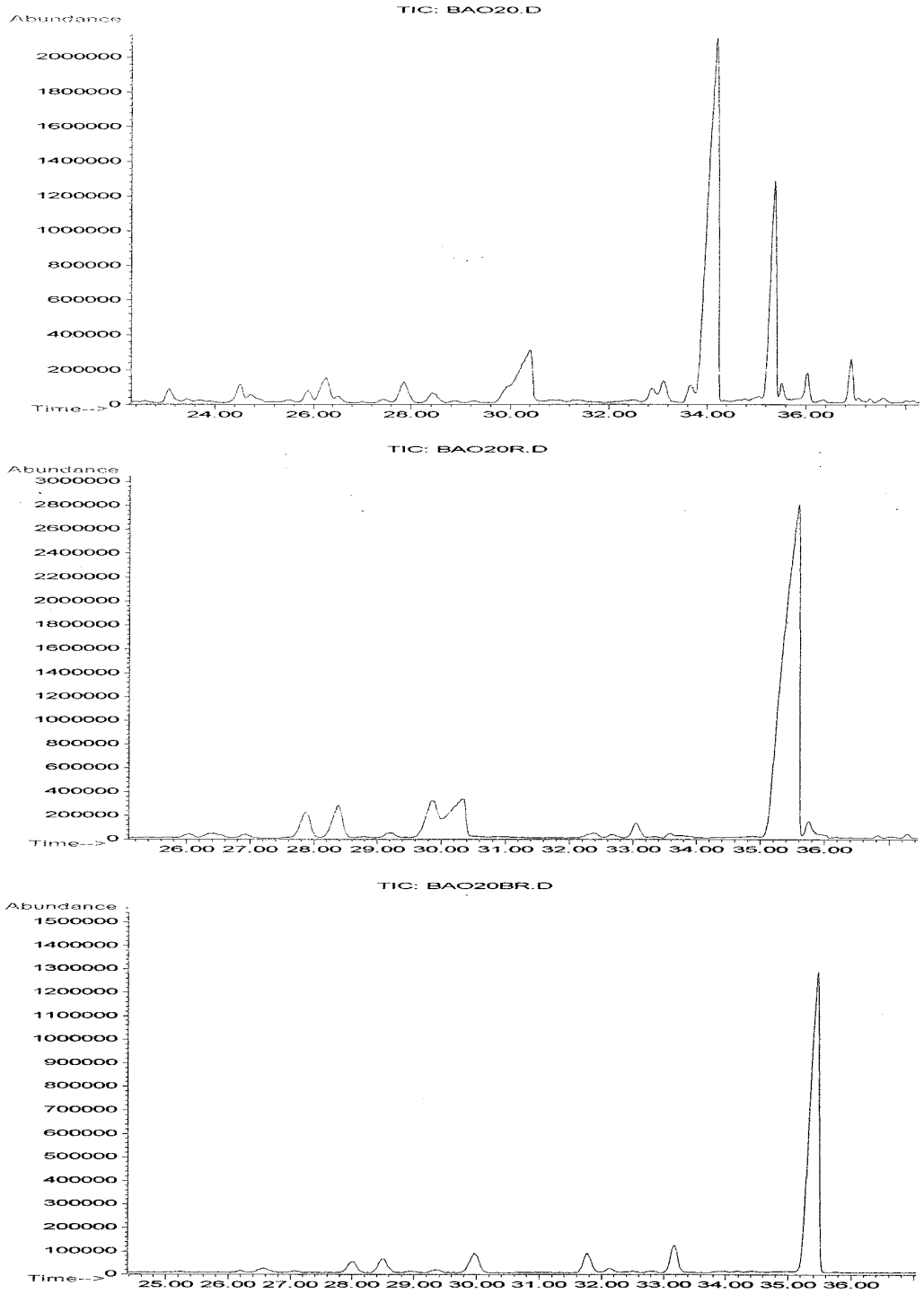

Figure 4. The Chromatogram of the Carbon-9 of the Run Bao20 (Top: FT products; Middle: after hydrogenation; Bottom: after bromination).

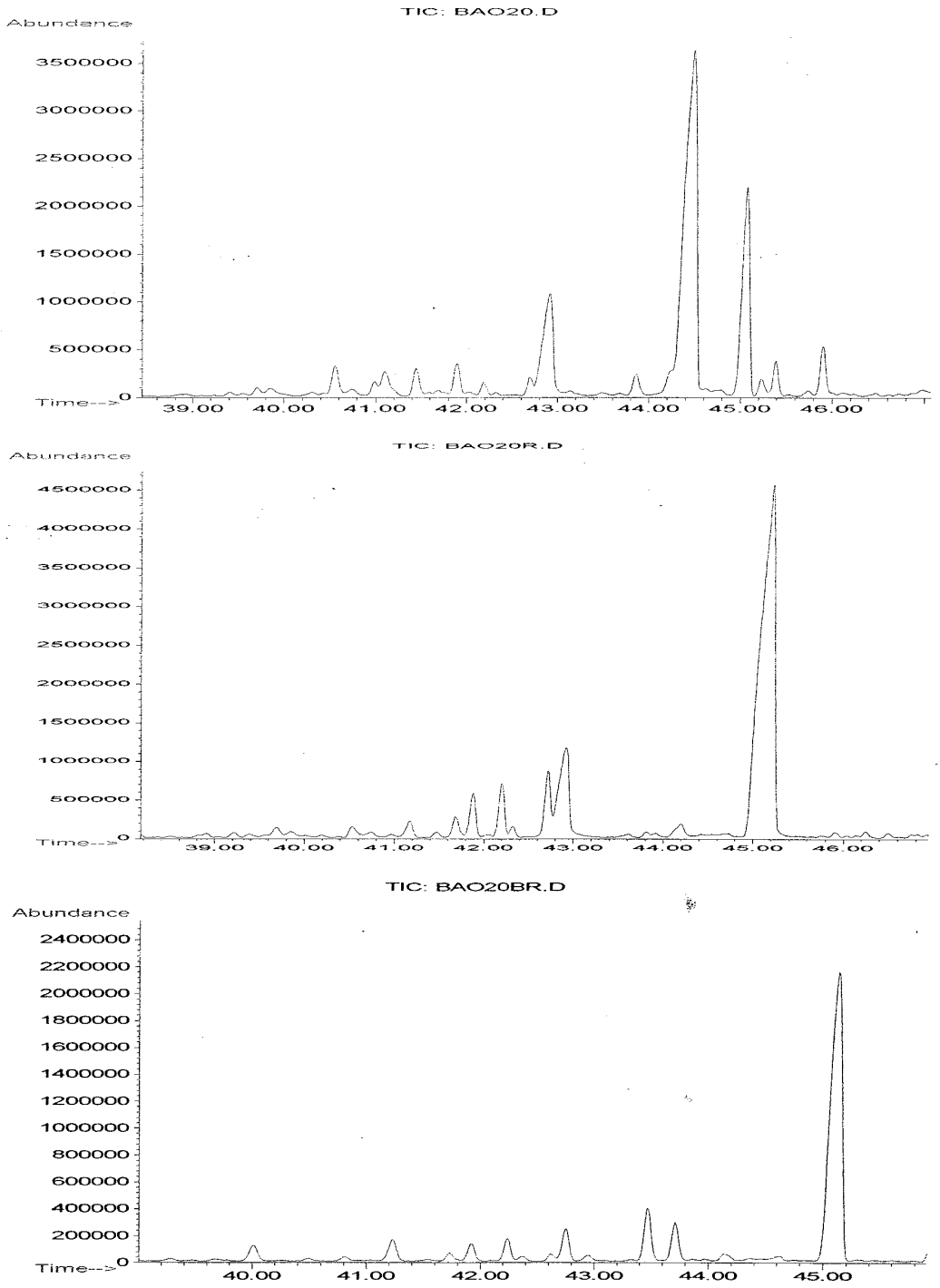

Figure 5. The Chromatogram of the Carbon-10 of the Run Bao20 (Top: FT products; Middle: after hydrogenation; Bottom: after bromination).

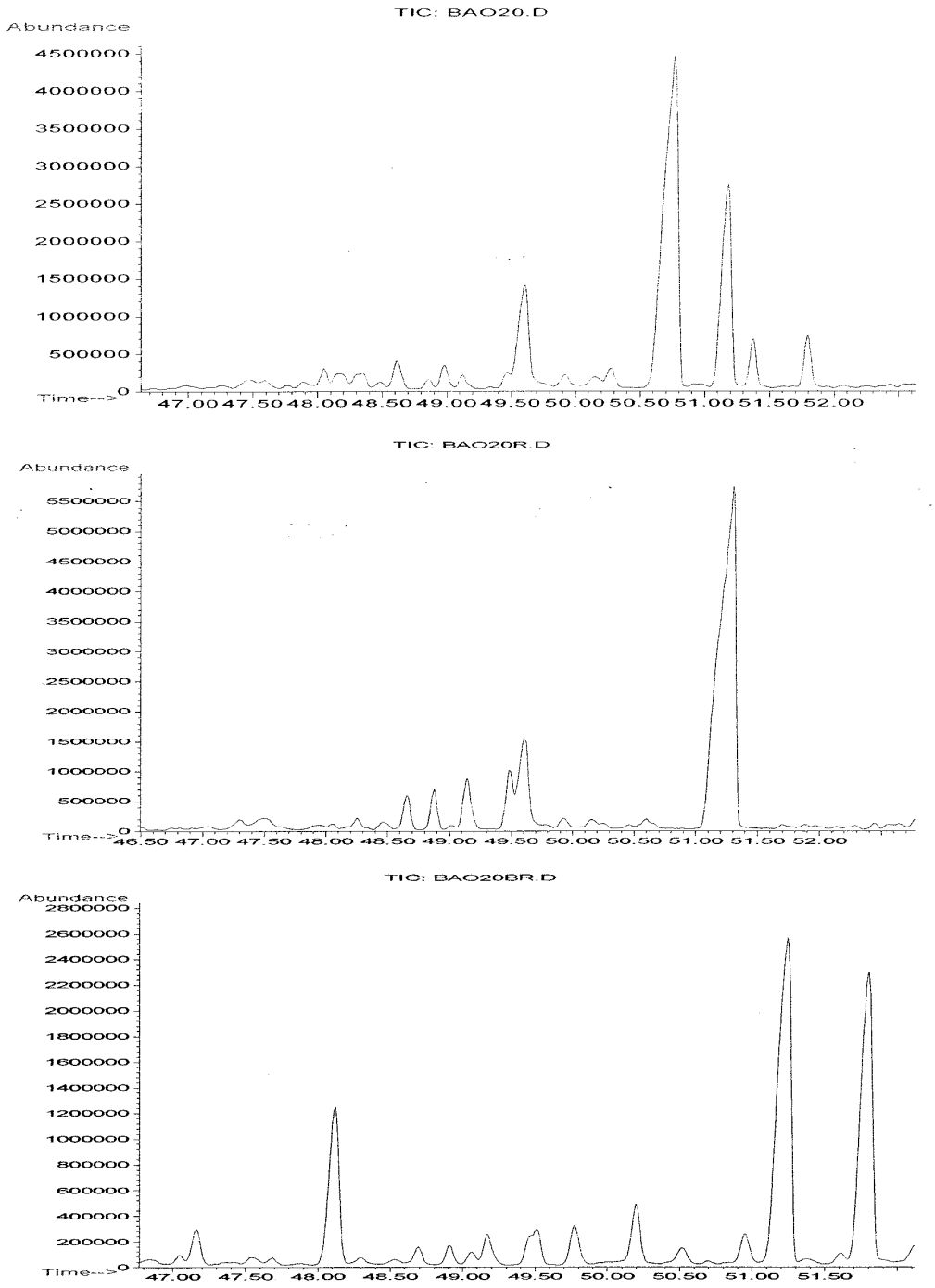

Figure 6. The Chromatogram of the Carbon-11 of the Run Bao20 (Top: FT products; Middle: after hydrogenation; Bottom: after bromination).

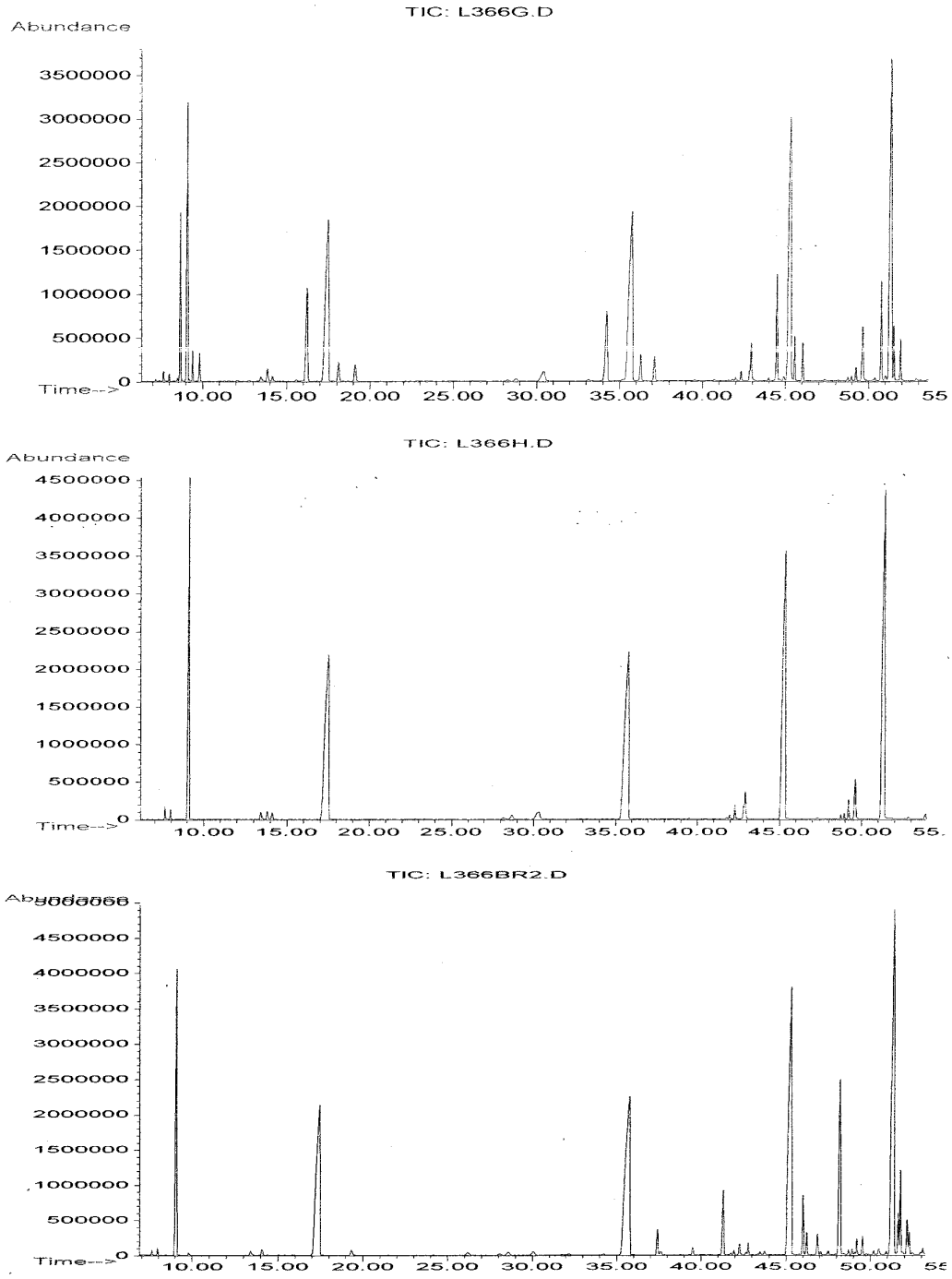

Figure 7. The Partial Chromatogram of the Oil Sample from Co Catalyzed FT reaction (Run ID: L366) (Top: FT products; Middle: after hydrogenation; Bottom: after bromination).

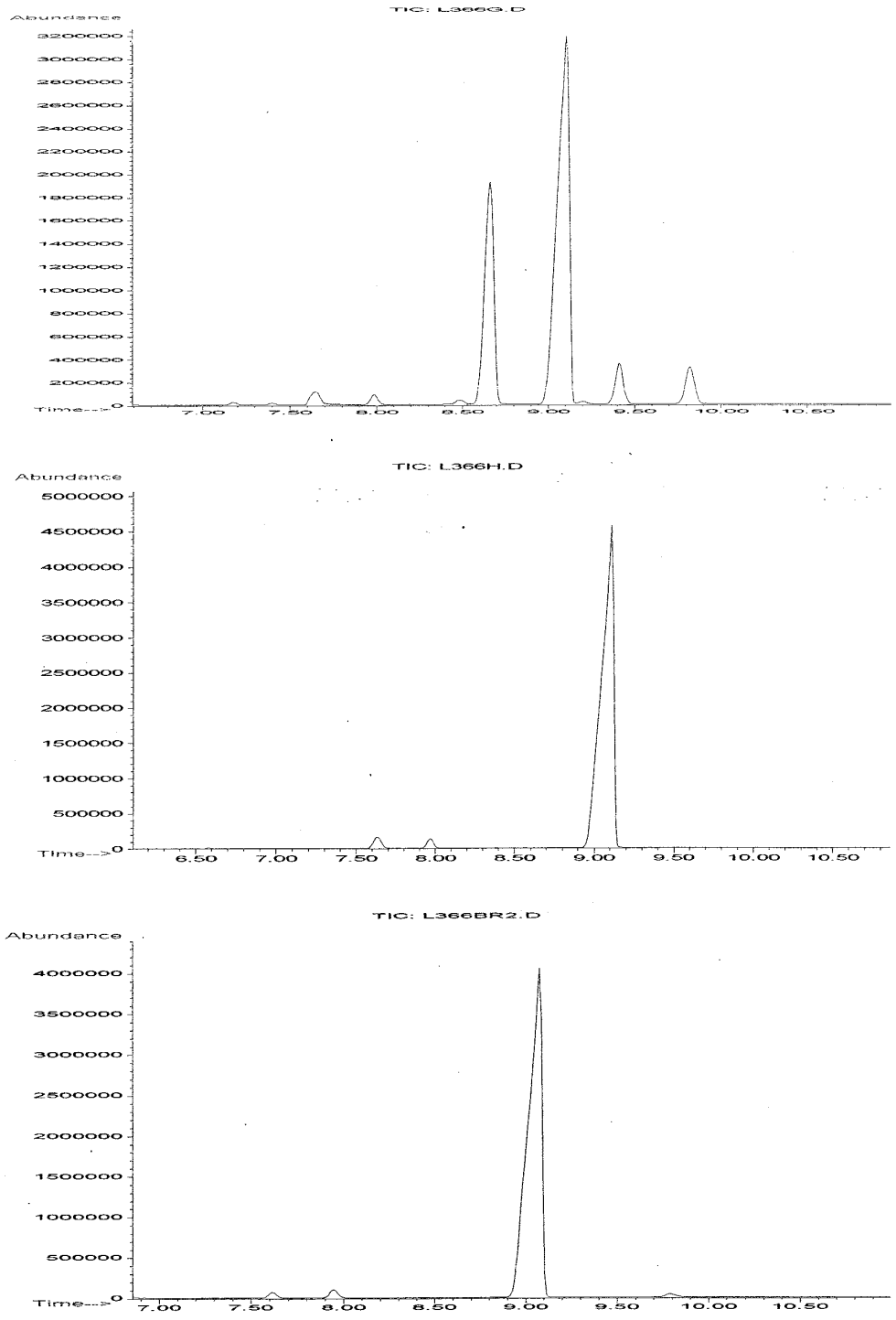

Figure 8. The Chromatogram of the Carbon-7 of the Run Bao20 (Top: FT products; Middle: after hydrogenation; Bottom: after bromination).

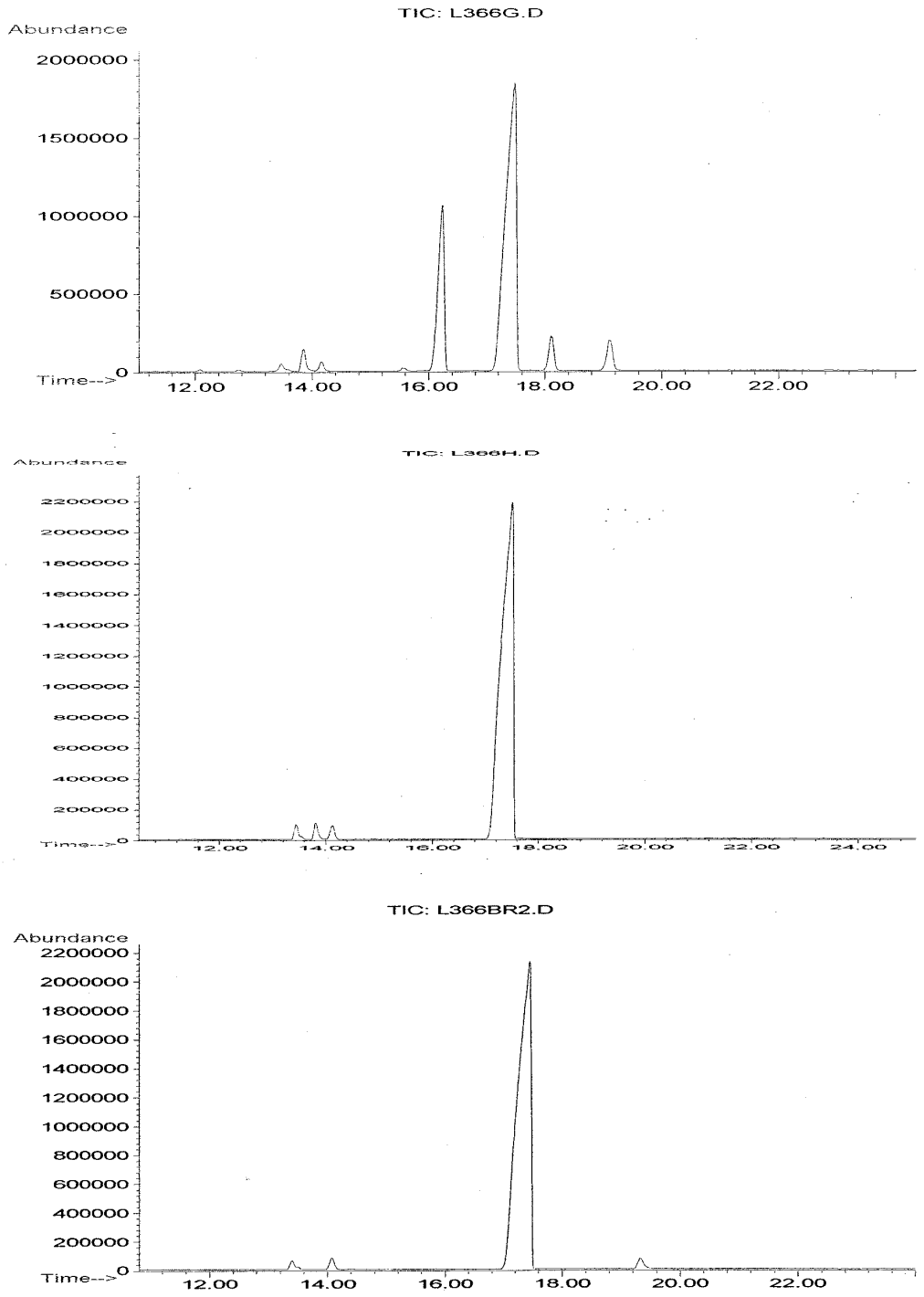

Figure 9. The Chromatogram of the Carbon-8 of the Run Bao20 (Top: FT products; Middle: after hydrogenation; Bottom: after bromination).

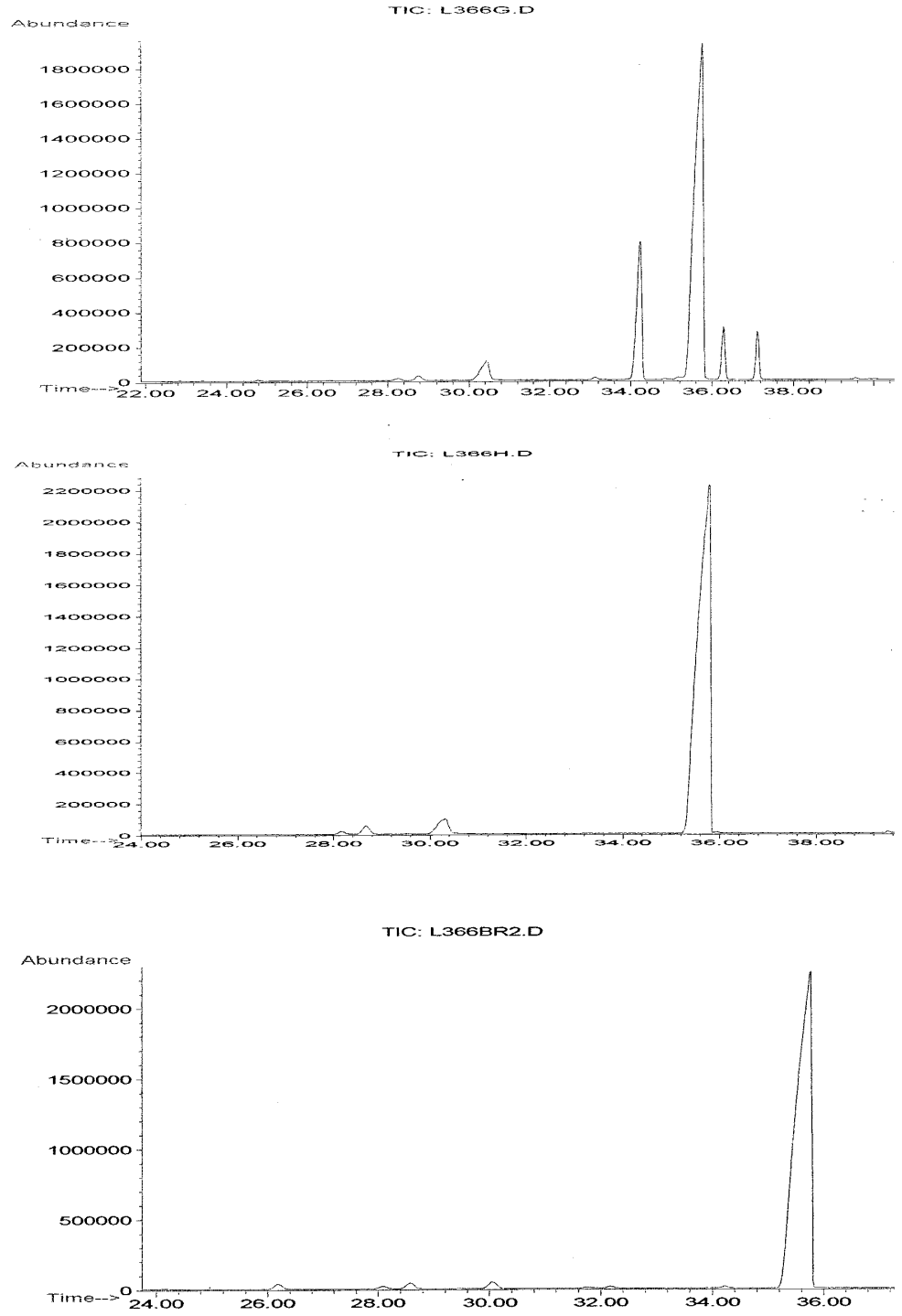

Figure 10. The Chromatogram of the Carbon-9 of the Run Bao20 (Top: FT products; Middle: after hydrogenation; Bottom: after bromination).

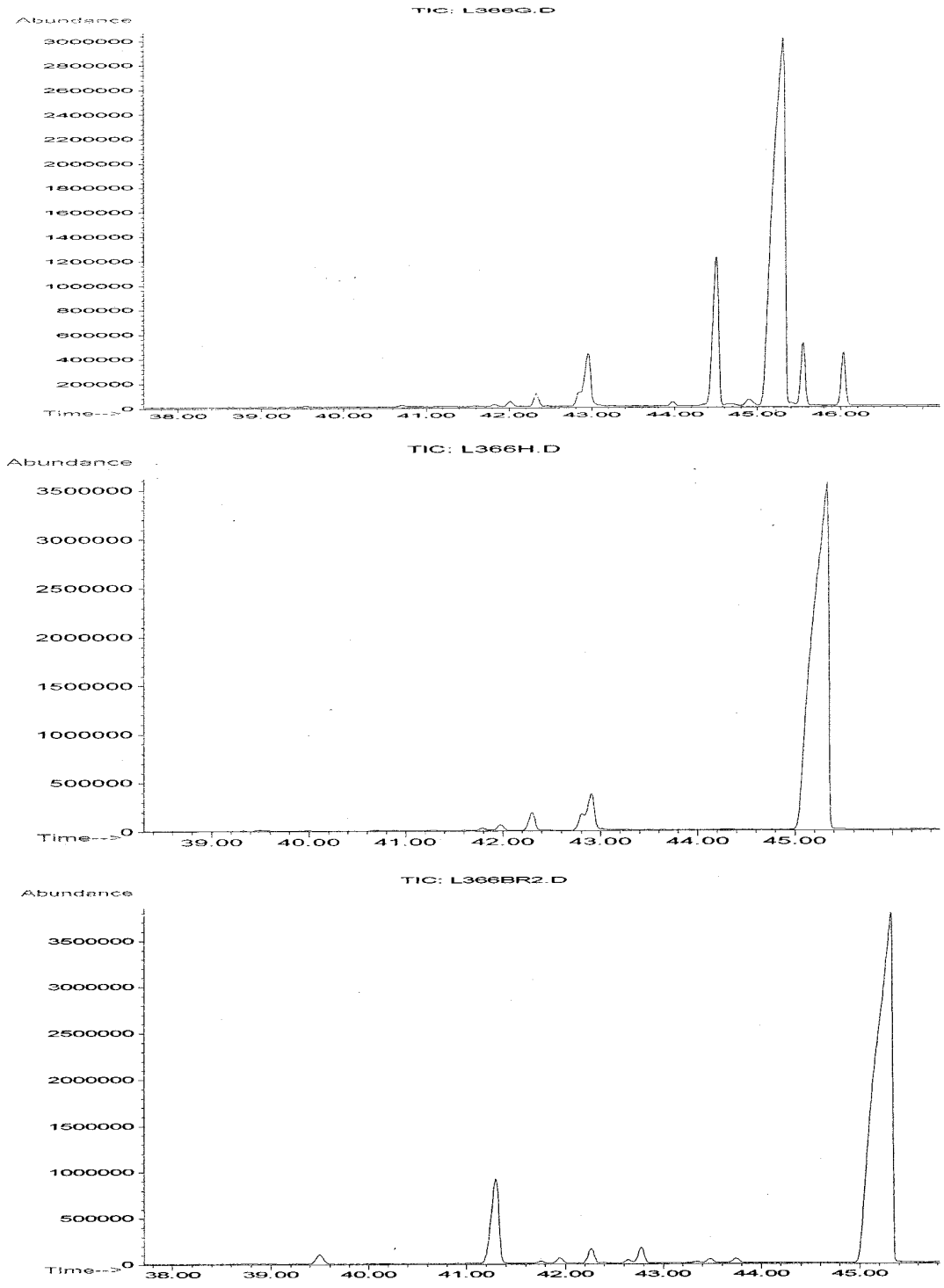

Figure 11. The Chromatogram of the Carbon-10 of the Run Bao20 (Top: FT products; Middle: after hydrogenation; Bottom: after bromination).

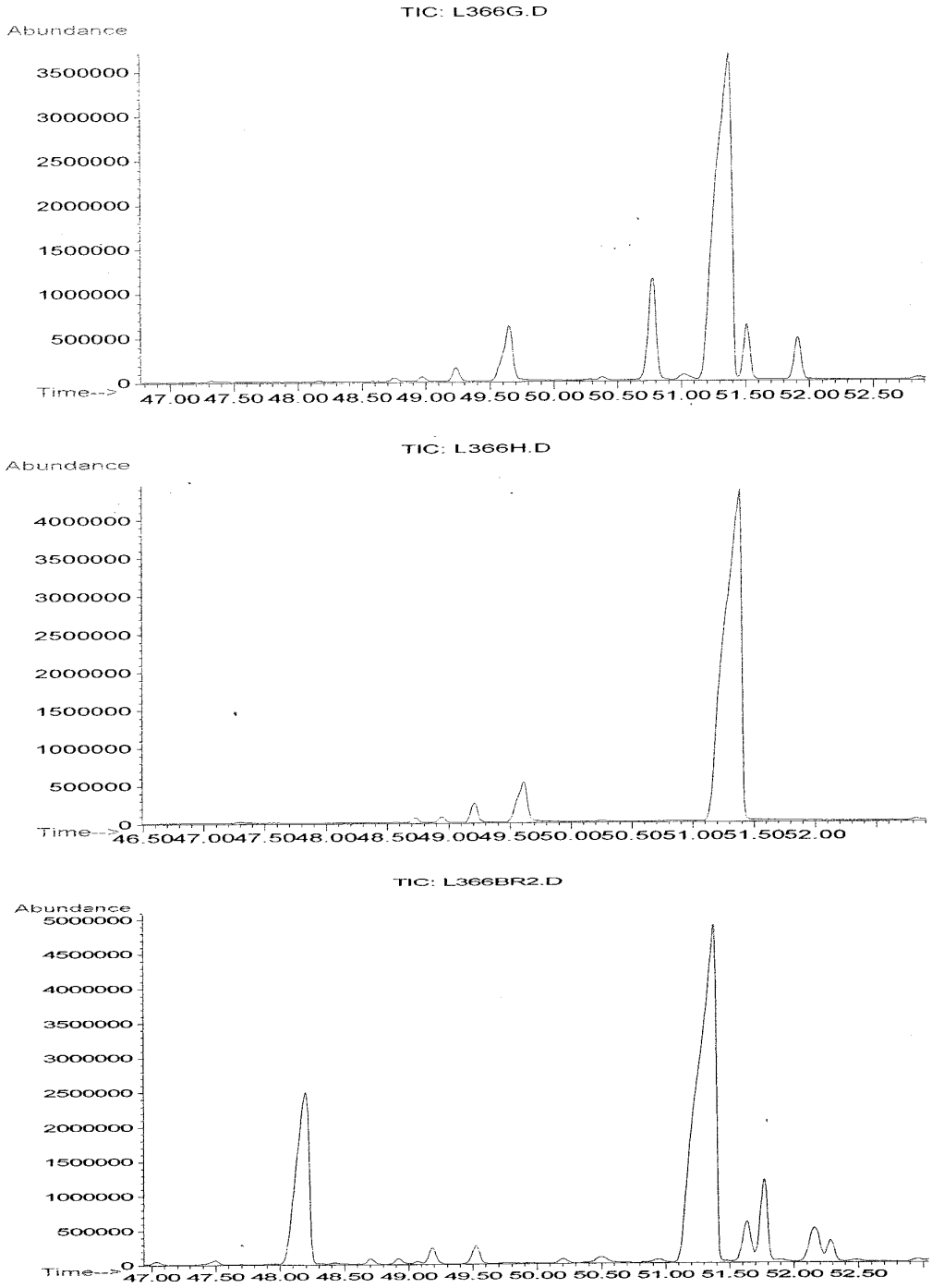

Figure 12. The Chromatogram of the Carbon-11 of the Run Bao20 (Top: FT products; Middle: after hydrogenation; Bottom: after bromination).

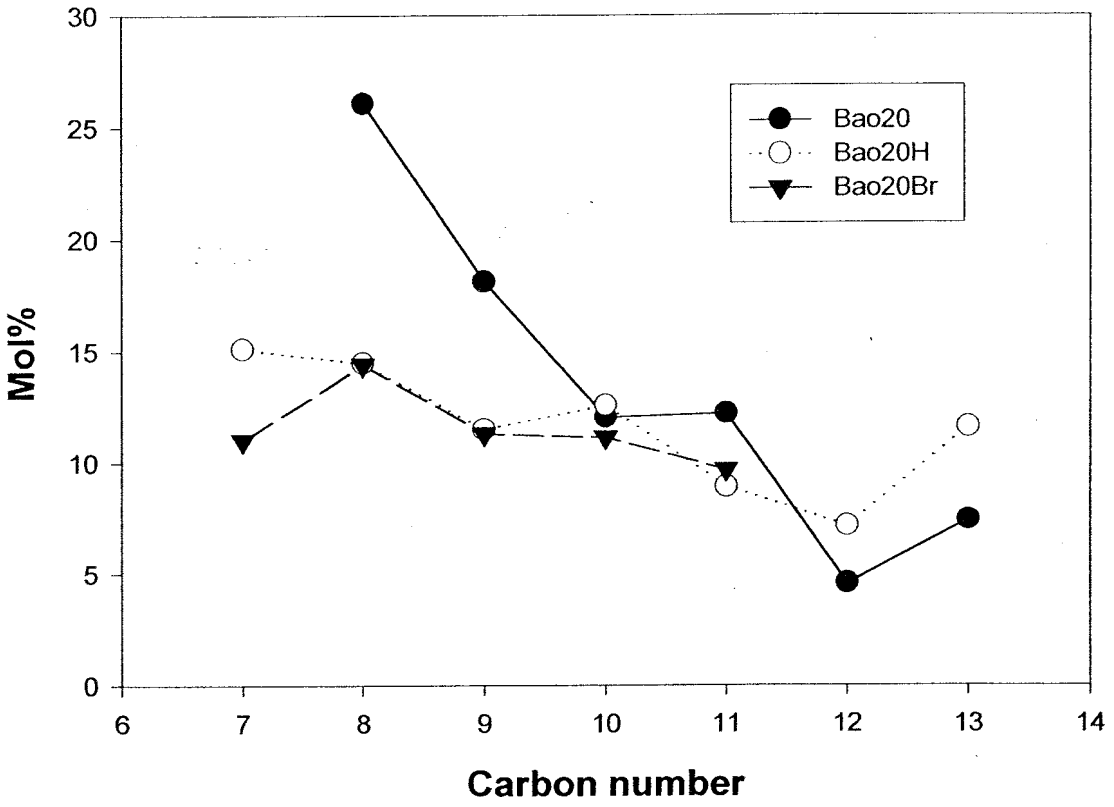

Figure 13. The Mole Percent of Branched Alkanes in Fe Catalyzed FT Products (Run ID: Bao20).

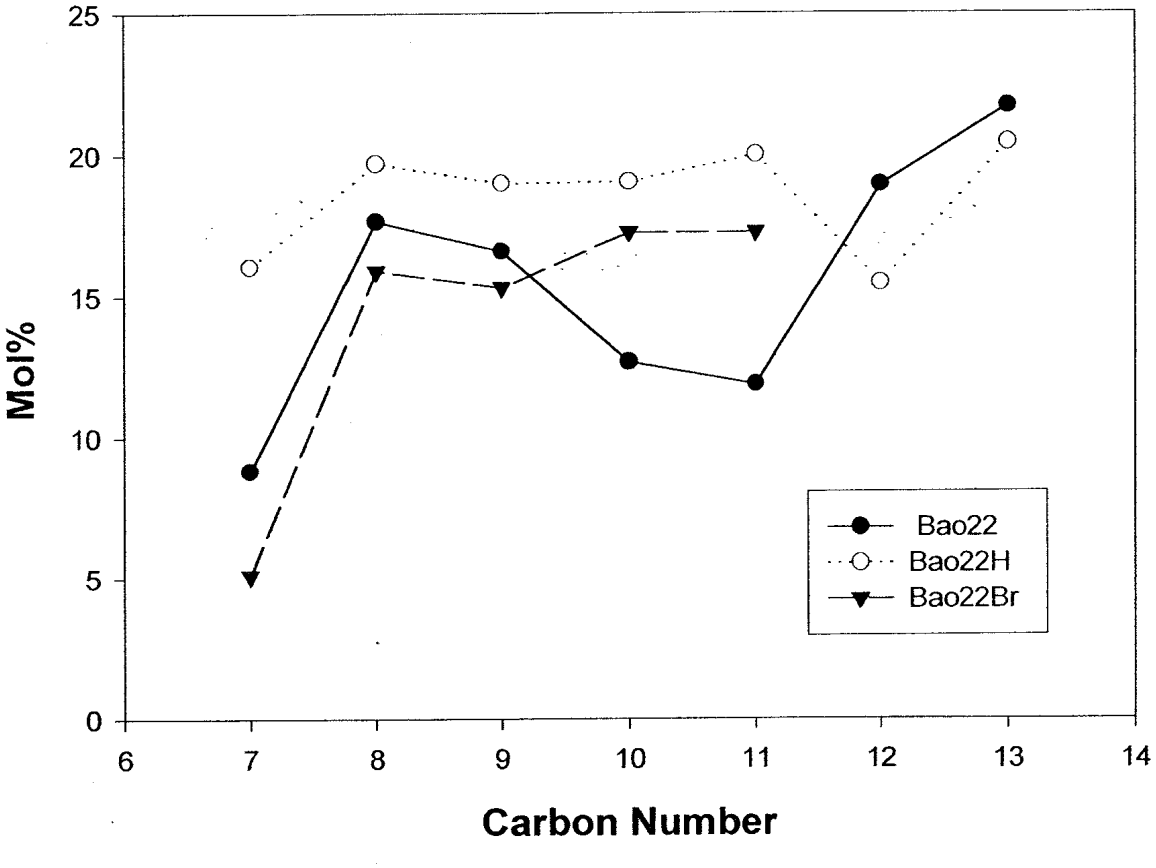

Figure 14. The Mole Percent of Branched Alkanes in Fe Catalyzed FT Products (Run ID: Bao22).

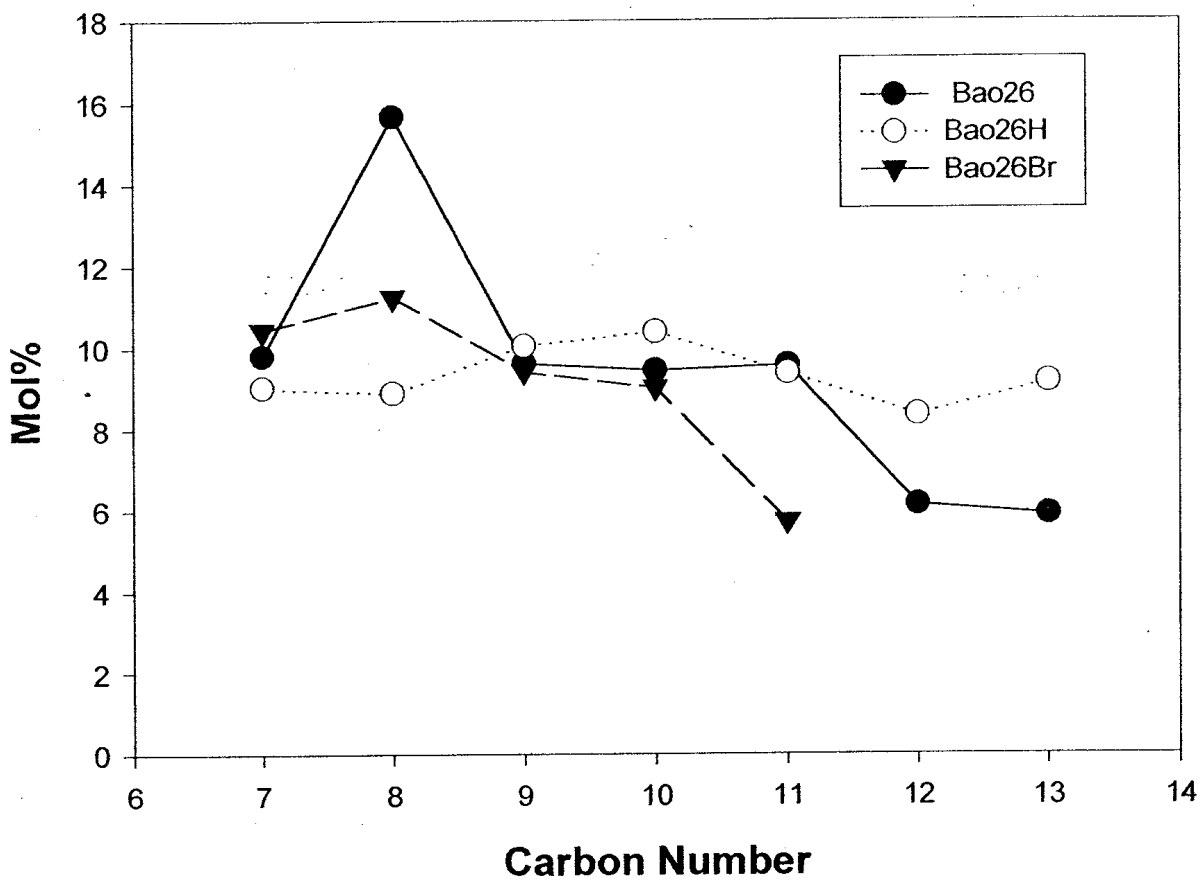

Figure 15. The Mole Percent of Branched Alkanes in Fe Catalyzed FT Products (Run ID: Bao26).

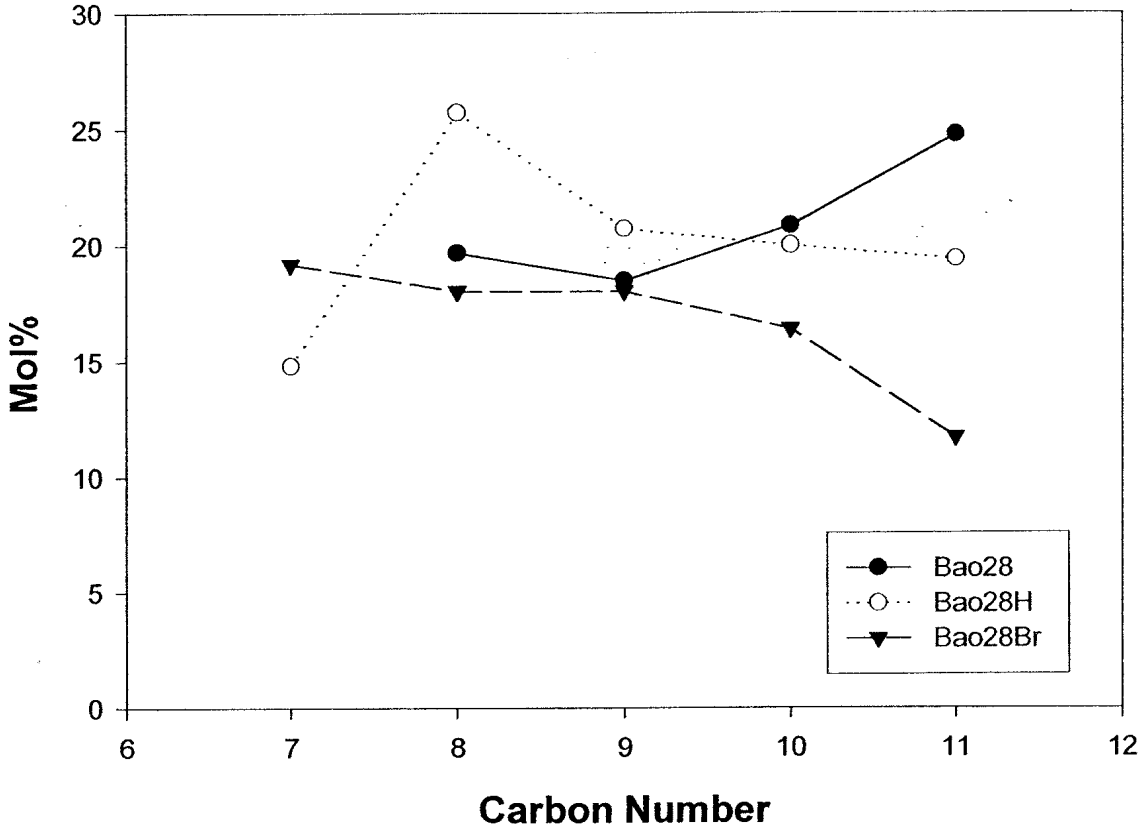

Figure 16. The Mole Percent of Branched Alkanes in Fe Catalyzed FT Products (Run ID: Bao28).

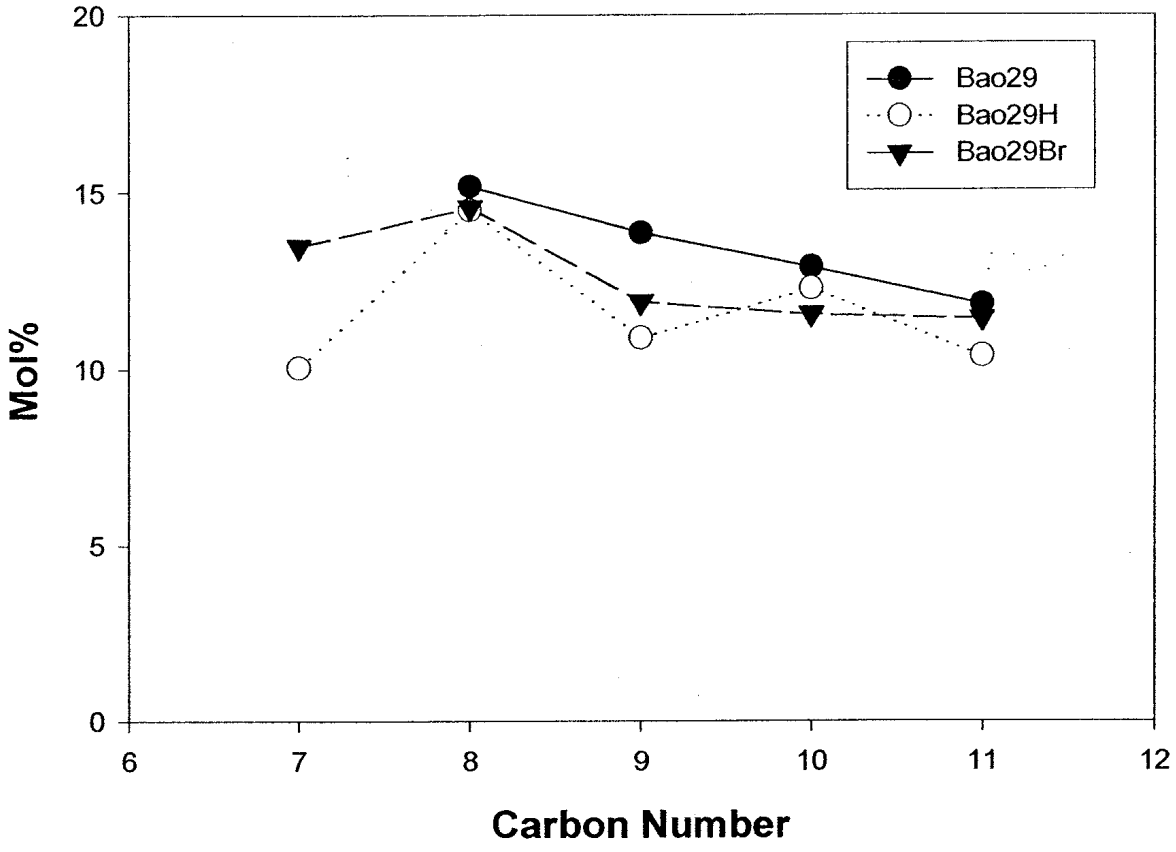

Figure 17. The Mole Percent of Branched Alkanes in Fe Catalyzed FT Products (Run ID: Bao29).

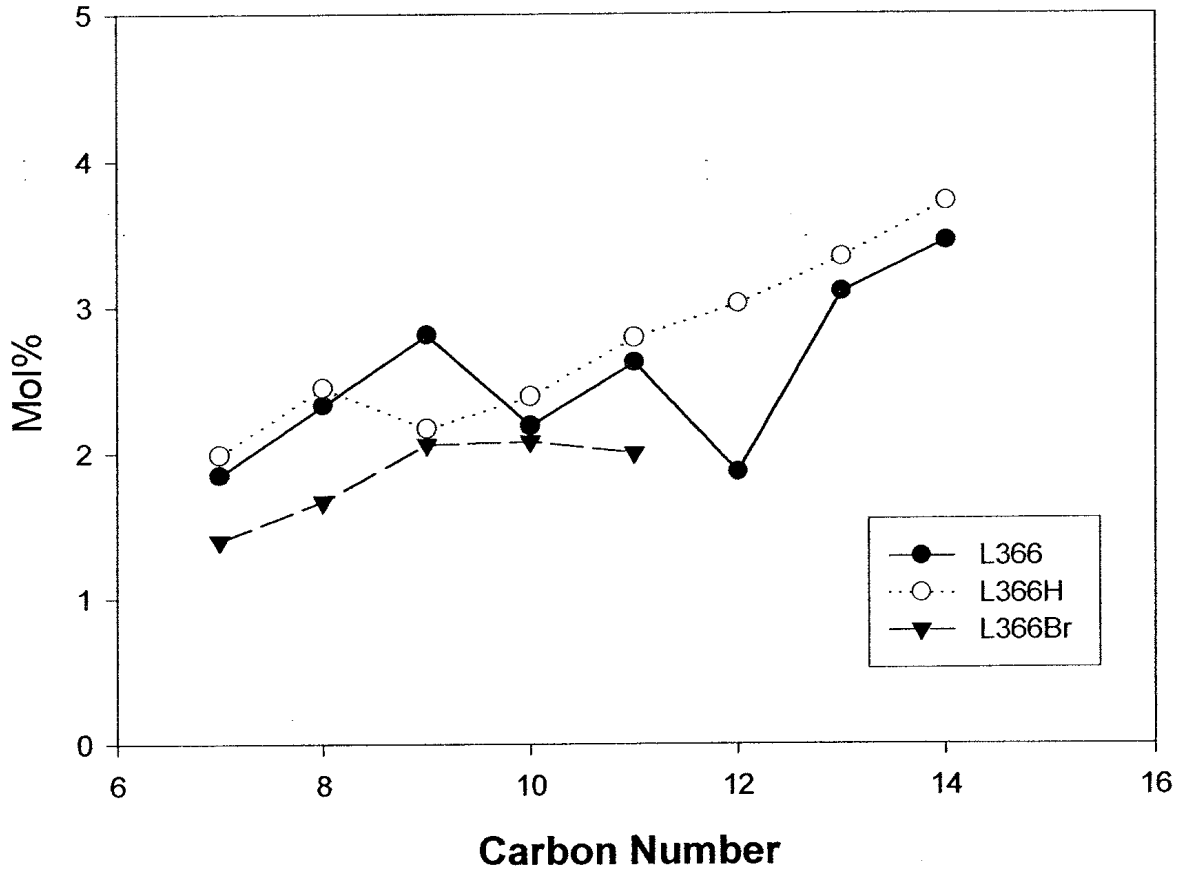

Figure 18. The Mole Percent of Branched Alkanes in Co Catalyzed FT Products (Run ID: L366).

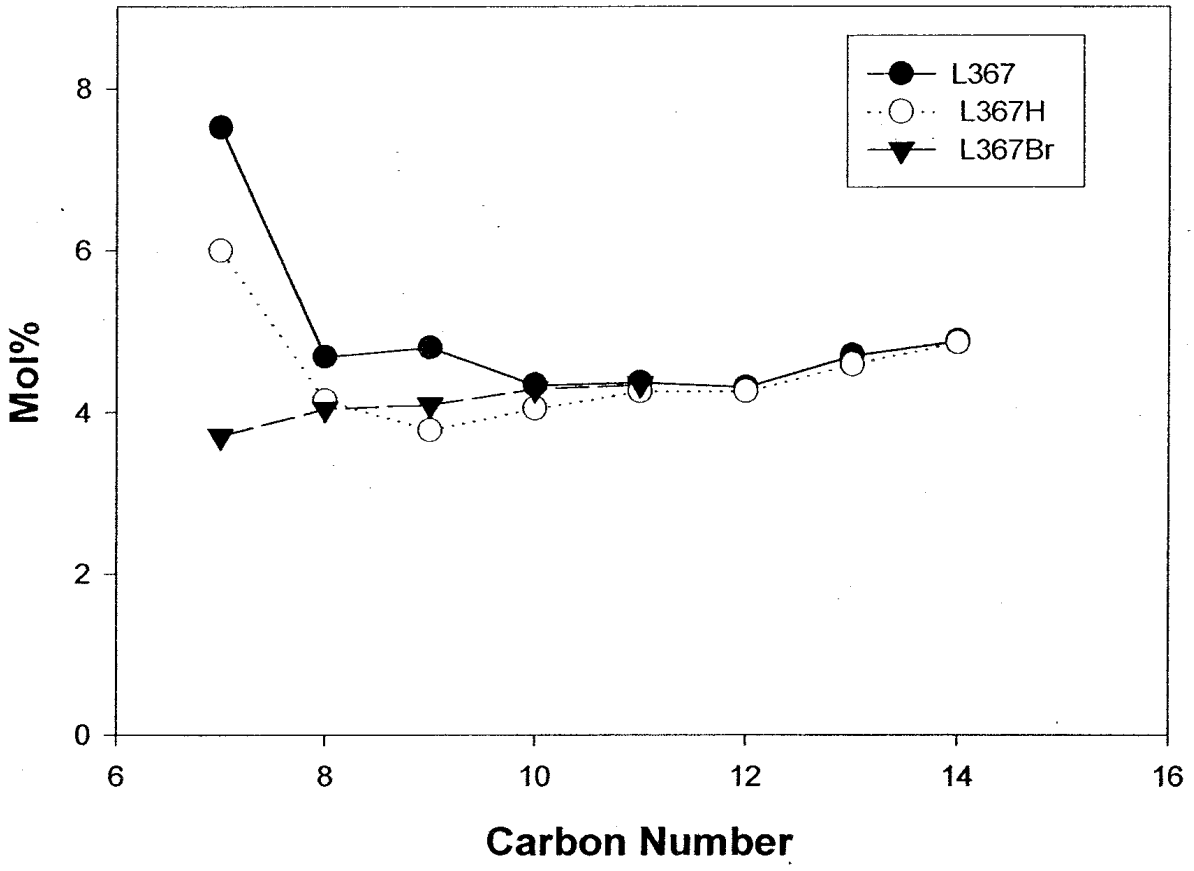

Figure 19. The Mole Percent of Branched Alkanes in Co Catalyzed FT Products (Run ID: L367).

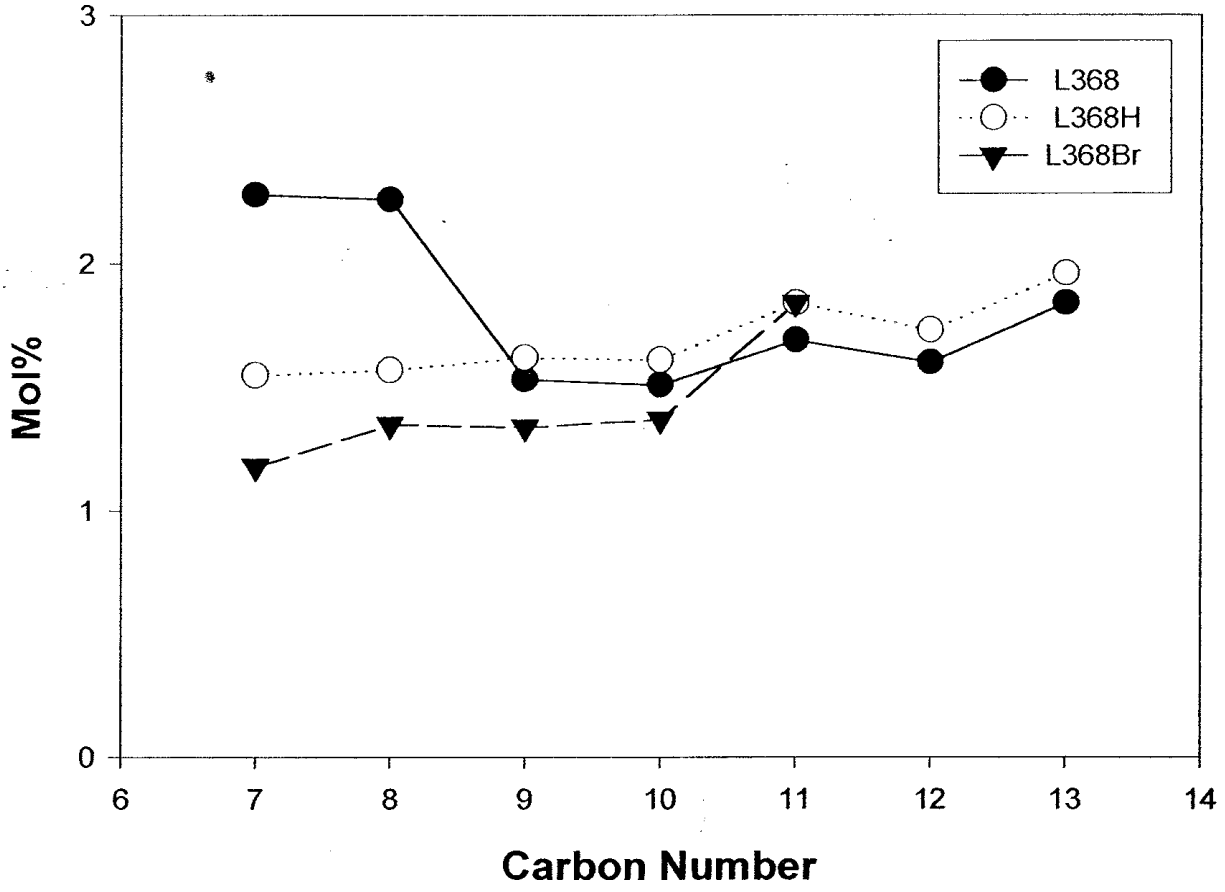

Figure 20. The Mole Percent of Branched Alkanes in Co Catalyzed FT Products (Run ID: L368).

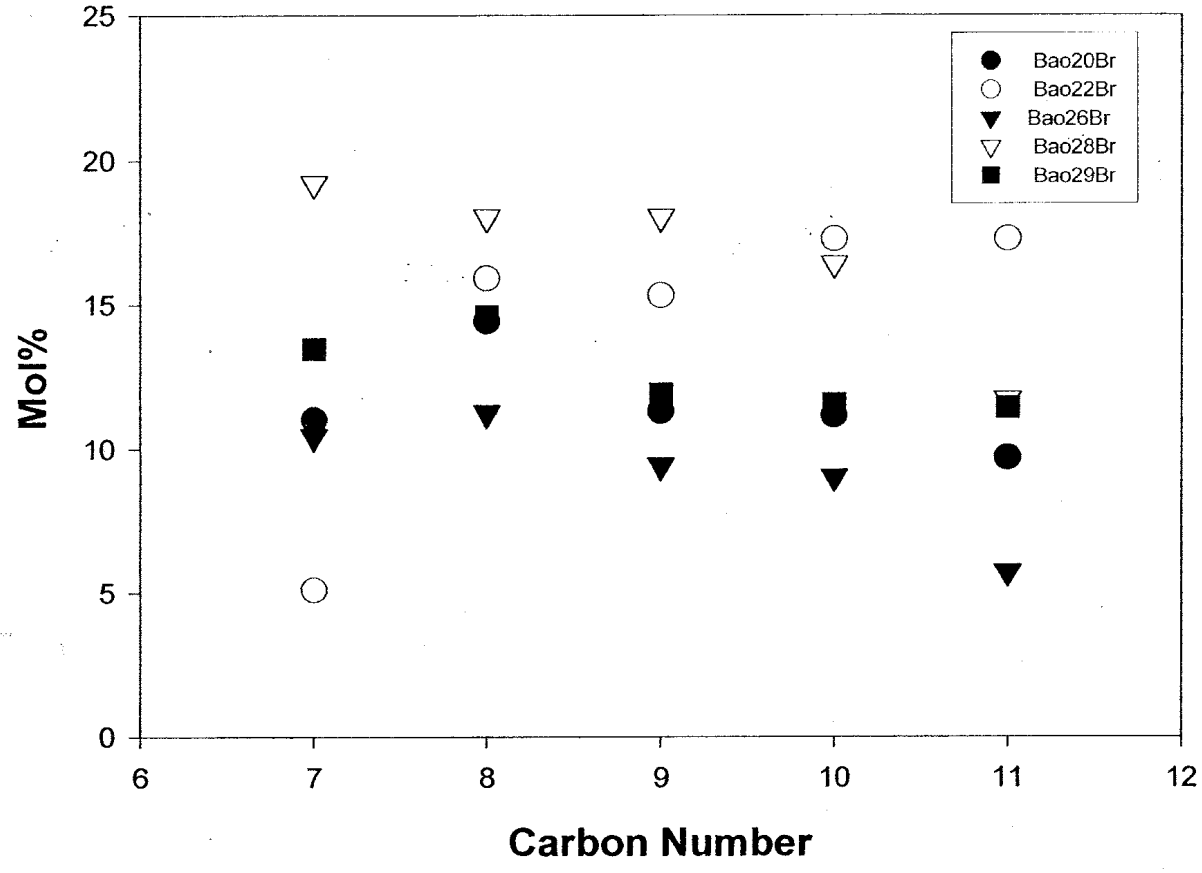

Figure 21. The Mole Percent of Branched Alkanes in Fe Catalyzed FT Products (after bromination).

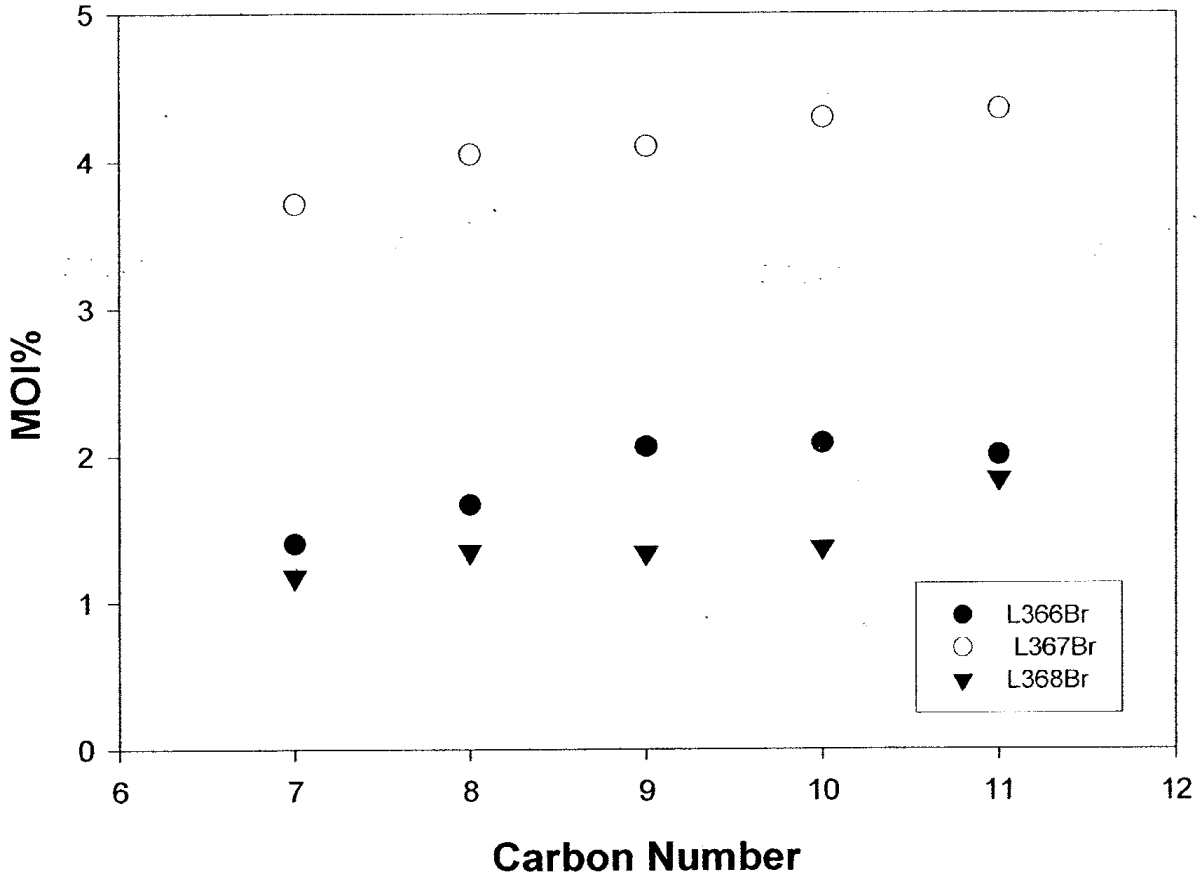

Figure 22. The Mole Percent of Branched Alkanes in Co Catalyzed FT Products (after bromination).

Task 3. Catalyst Characterization

The objective of this task is to obtain characterization data of the prepared catalysts using routine and selected techniques.

The chemisorption apparatus has been installed. Characterization of cobalt catalysis is underway.

Task 4. Wax/Catalyst Separation

The objective of this task is to develop techniques for the separation of catalysts from FT reactor slurries.

A. Hi-alpha Catalyst and Special Filter

Today, the marketplace place a premium on FTS diesel but not gasoline; thus, the current view is that the most attractive option is to produce high molecular wight FTS products and then to hydrocrack them to produce high quality diesel fuel. High molecular weight FTS products are not volatile at the usual reaction temperatures and pressure. This requires that liquid products be separated from the catalyst.

The inability to operate the fixed-bed reactor isothermally makes it attractive to use a slurry bubble column reactor. With the slurry reactor, a wax-catalyst separation must be accomplished, either within or external to the reactor.

This report presents the preparation of three of high alpha iron catalysts that can produce large quantities of high molecular weigh FTS products and four filters to be used for wax-catalyst separation within the slurry reactor.

100Fe/4.6Si (Atomic ratio) is prepared by dissolving Fe $(NO_3)_3 \cdot 9H_2O$ (18907.29 g) and tetraethyl orthosilicate (448.76 g) in distilled water, then precipitated with concentrated ammonium hydroxide. The pH of the slurry was >9 . The slurry was filtered. The filter cake was

dried at 110˚C. The base catalyst was crushed to approximately 60μm and calcined in air at 350˚C for 4hr.

The 100Fe/4.6Si bade catalyst was impregnated with the appropriate amount of K_2CO_3 and Cu $(NO_3)_2 \cdot 3H_2O$ to give an atomic composition of 100 Fe/4.6Si/2.0Cu/5K, 100Fe/4.6Si/2.0Cu/7.5K and 100Fe/4.6Si/2.0Cu/10k. The amount of K_2CO_3 and Cu $(NO_3)_2 \cdot 3H_2O$ added will depend on the iron content of base catalyst. Typically the base catalyst is about 68 wt% Fe. For an atomic composition of 100/Fe/4.6Si//2.0Cu/7.5K, 80.05g of 100 Fe/4.6Si was impregnated with 26.4 ml of an aqueous Cu $(NO_3)_2 \cdot 9H_2O$ (17.8289 g Cu $(NO_3)_2 \cdot 9H_2O$ Per 100ml solution). Following the impregnation the catalyst was dried at 110˚C with good mixing. The same procedure was used to add K. It was impregnated with 26.4ml of a K_2CO_3 solution (5.0484 g K_2CO_3 per 50ml solution). The catalyst was dried at 110˚C with good mixing.

Approximately 32.22g of catalyst (100Fe/4.6Si/2.0Cu/5K, 100Fe/4.6Si/2.0Cu/7.5K or 100Fe/4.6Si/2.0Cu/10K), respectively, and 310g Ethylflo 164 oil (C_{30}) were loaded into a 1-liter stirred autoclave reactor. The slurry was treated with carbon monoxide at 40 Lh^{-1} at 1.31MPa pressure; the temperature was then increased to 270ºC at 120ºCh^{-1} and held at this temperature for 24h. The temperature was reduced to 230ºC. CO flow was decreased and hydrogen flow gradually increased until the total flow was 3 SL/gFe/hr. The ratio of H_2 and CO is 0.7.

These catalysts (100Fe/4.6Si/2.0Cu/5K, 100Fe/4.6Si/2.0Cu/7.5K and 100Fe/4.6Si/2.0Cu/10K) have very low methane production and high alpha value (see Table 1). That means these catalyst produce a large amount of high molecular weight FTS products (reactor wax).

The main purpose for running these catalysts was to test whether these four filters possess sufficient ability to remove reactor wax from reactor, and whether these filter have enough ability to separate reactor wax from iron catalyst. Running conditions and filter specification are given in Table 2.

Carbon monoxide conversion for each high-alpha catalyst is shown in Figure 1. The 100Fe/4.6Si/2.0Cu/7.5K catalyst had the highest conversion. The catalysts went through an induction period in which the conversion increased from about 10 to 43 %. These high-alpha catalysts have sufficient activity at 230^{o}C for FTS.

The alkene selectivities, as a function of carbon number, are similar for the three high-alpha catalysts (Figures 2-4). These three high-alpha catalysts produce more alkene than the lower atomic K% catalysts.

During 1000 hrs. of run time, the amounts of reactor wax removed from the reactor are 1800g, 2000g, 1500g and 1200g for 100Fe/4.6Si/2.0Cu/5K, 100Fe/4.6Si/2.0Cu/7.5K, and 100Fe/4.6Si/2.0Cu/10K catalysts, respectively (Figures 5-8). The reactor wax removed from the reactor depend on potassium content of the catalyst, and during this time does not depend on the filter surface area and pore size. These filters, compared with the 2 micro sinter metal filters (used from 1991 until now for removing reactor wax) posses ability to remove reactor wax for high-alpha catalysts. For example, during a 100 hr run, using 100Fe/4.6Si/2.0Cu/10K high-alpha catalyst, we were able to remove only 5g of reactor wax form the CSTR but with these special filters we can remove about 120g.of reactor wax from CSTR each day. Filtration data for these filters are shown in Table 3.

For special filter, 1.8-2.1 g of iron (about 8–9.6 % of iron) is lost after 1000 hr running (Figures 9 and 10). Much of this iron (20-30%) is lost during the period of cake build-up and can be eliminated by engineering design.

In summary, these catalysts have sufficient activity to merit consideration for producing high molecular weight FTS products and the preliminary data using the filters suggest that they may have sufficient ability to remove reactor wax form CSTR.

Table 1

CH_4 Selectivity and Alpha Value

Run No.	Average CH_4 Selectivity	α_1	α_2
Bao035	1.60	0.68997	0.91438
Bao036	1.50	0.73293	0.91468
Bao041	1.50	0.71138	0.92363
Bao043	1.70	0.76618	0.90876

Table 2

General Information

Run No.	Catalyst	Reactor Temp, °C	Reactor Pressure (psig)	Filter Length (inch)	Filter Diameter (inch)	Filter Surface Area $(inch)^2$	Pore Size
Bao035	100Fe/4.61Si /2.0Cu/5K	230	175	0.5	1	1.57	2μ
Bao036	100Fe/4.6Si/ 2.0Cu/5K	230	175	0.5	1	1.57	18μ
Bao041	100Fe/4.6Si/ 2.0Cu/7.5K	230	175	1.0	1	3.14	18μ
Bao043	100Fe/4.6Si/ 2.0Cu/10K	230	175	1.5	1	4.71	18μ

Table 3

Filtration of Bao041 (Filter L = 1"; reactor pressure = 175 psig; pressure of rewax trap set = 125 psig)

Number	Time Sample Taken (min.)	Amount of Wax Removed (g/5 min)
1	5	2.5
2	5	4.32
3	5	2.99
4	5	5.35
5	5	2.77
6	5	1.69
7	5	2.70
8	5	2.25
9	5	3.60
10	5	1.64

Figure 1. CO conversion Vs TOS at 230 ^{0}C

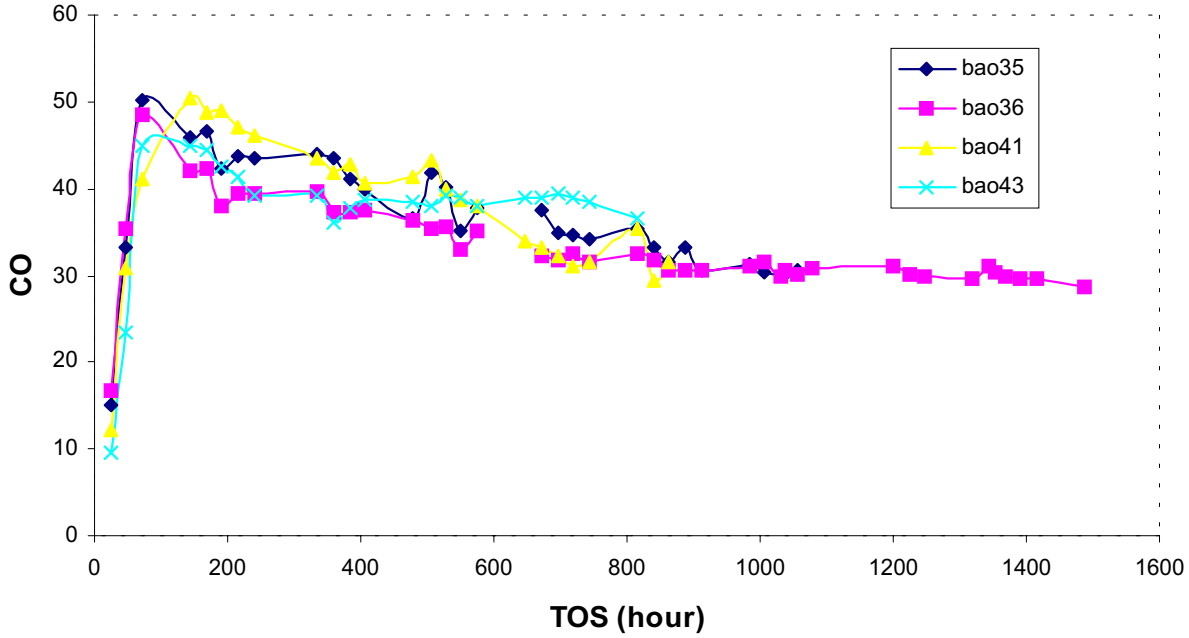

Figure 2. olefin/(olefin+paraffin) Vs.carbon number for the catalyst containg 5%K(Bao035

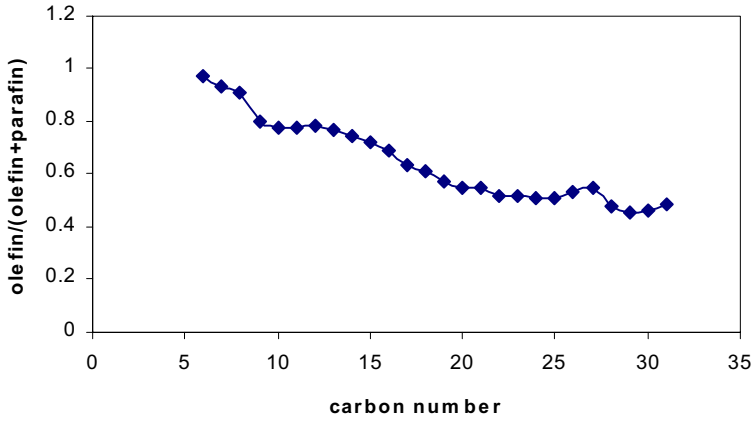

Figure 3. olefin/(olefin+paraffin) Vs. carbon number for the catalyst containg 7.5%K (Bao041)

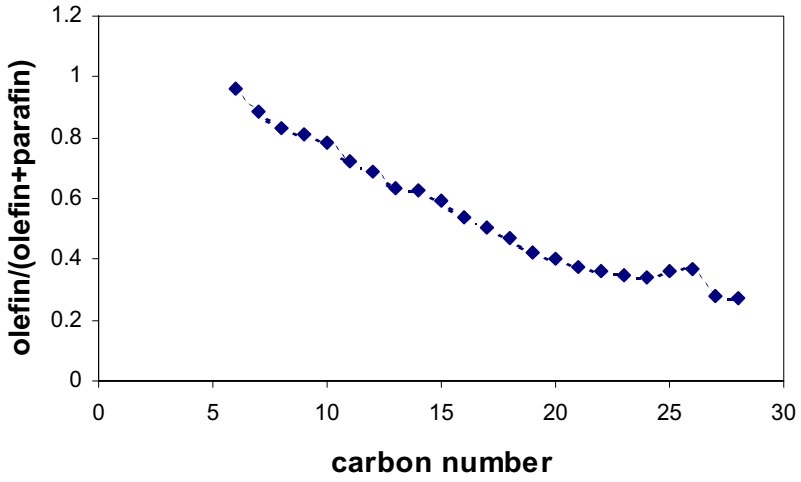

Figure 4. olefin/(olefin+paraffin) Vs. carbon number for catalyst containg 10%K (Bao043)

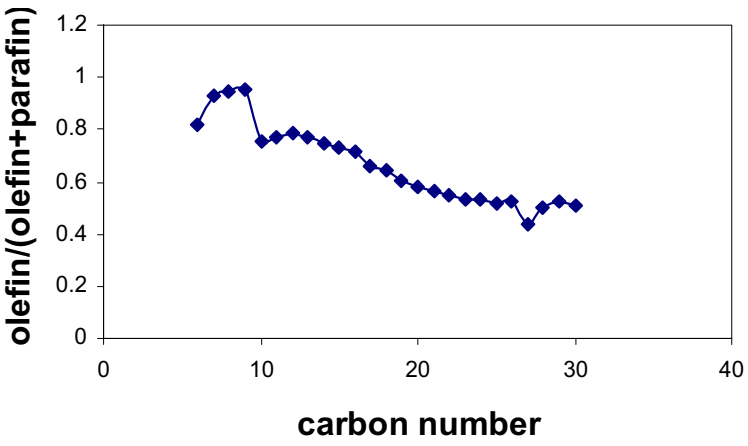

Figure 5 Cumulation Rewax Removal Vs. Time on stream for 100Fe/4.6Si/2.0Cu/5K Catalyst

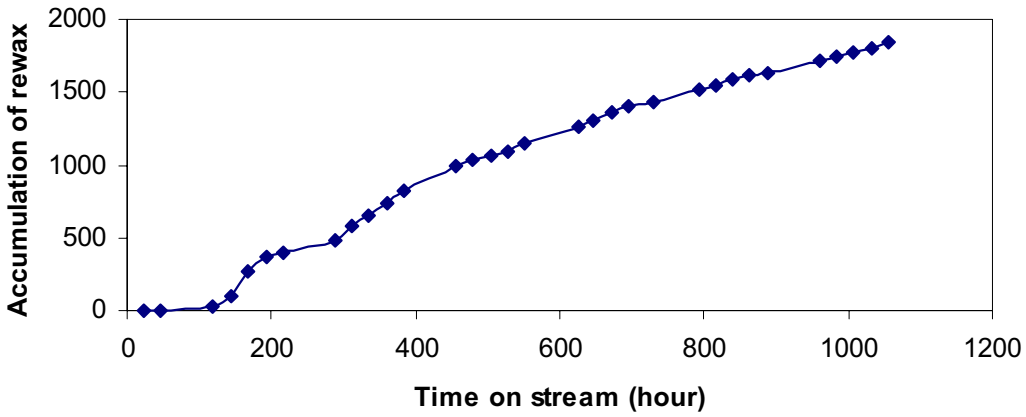

Figure 6 Cumulation Rewax Removal Vs. Time on stream for 100Fe/4.6Si/2.0Cu/5k Catalyst

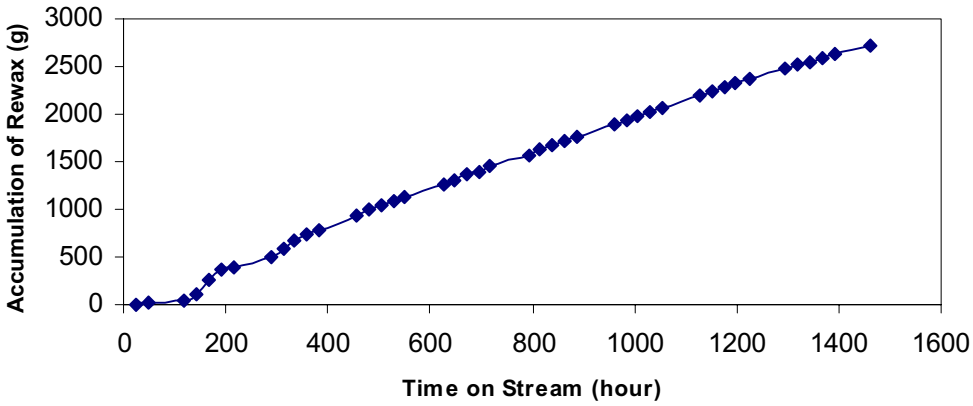

Figure 7. Cumulation Rewax Removal Vs.Time on stream for 100Fe/4.6Si/2.0Cu/7.5K

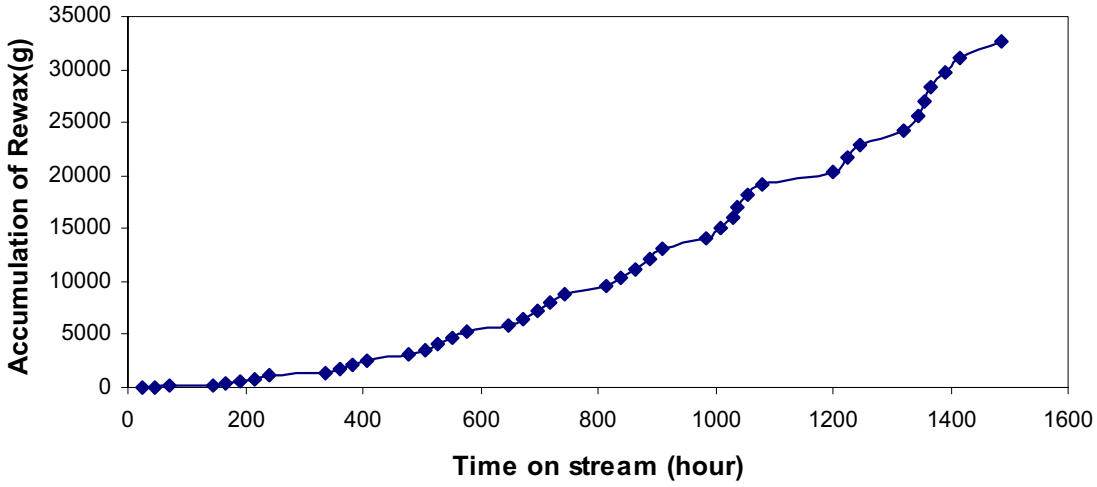

Figure 8. Cumulation Rewax Removal Vs.time on stream for 100Fe/4.6Si/2.0Cu/10K

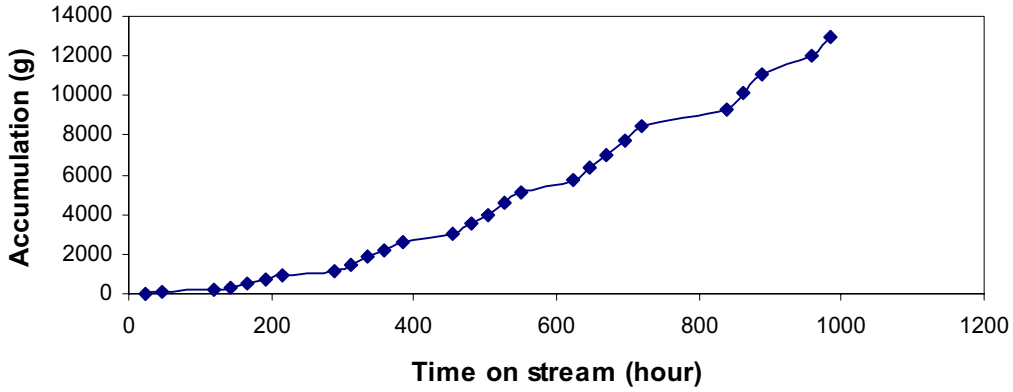

Figure 9 Cumulatial of iron Vs. time on stream for 100Fe/4.6Si/2.0Cu/5K Catalyst

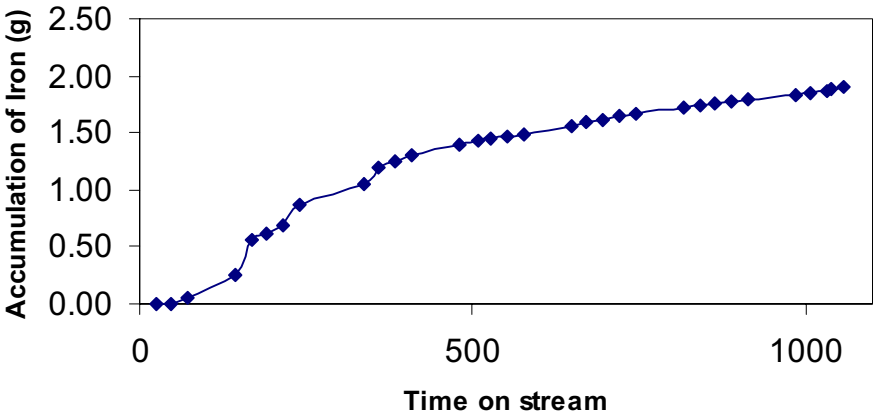

Figure 10 Cumulation of Iron Removal vs. time on stream for 100Fe/4.6Si/2.0Cu/5K Catalyst

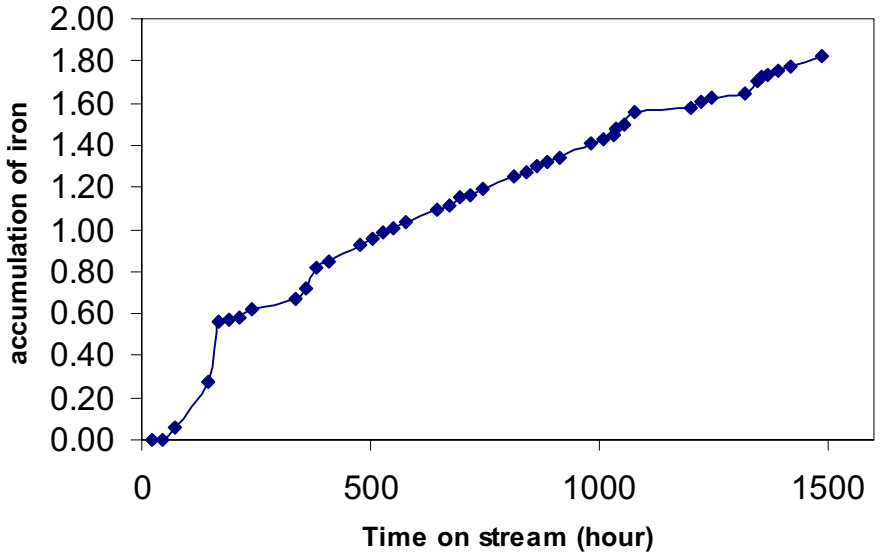

Task 5. Oxygenates

The objective of this task is to obtain a better understanding of the factors that affects catalyst selectivity toward oxygenates for iron-based Fischer-Tropsch catalysts.

Alcohol, aldehyde, ketene and acid standards were run on four different columns for evaluation and optimization of the separation of these compounds prior to the installation and analysis by the GC-AED. All the columns do not provide good chromatography for the free organic acids. A HP-INNOWAX column is currently being evaluated for their applicability for analysis of the free organic acids.

Runs in the CSTR using various alkali promoters (Li, Na, Rb and Cs) on the 100Fe/4.6Si base catalyst have been completed. These samples will be run in the GC-AED to analyze the individual oxygenates in the oil and wax sample to evaluate the effect of the promoters.

Task 6. Literature Review of Prior Fischer-Tropsch Synthesis with Co Catalysts

The objective of this task is to prepare a critical review of prior work on cobalt Fischer-Tropsch catalysts.

An extensive report has been submitted. Currently a review of the kinetics for iron and cobalt catalysts is underway.

Task 7. Co Catalyst Preparation

The objective of this task is to prepare a limited number of cobalt-based Fischer-Tropsch catalysts that can be used to obtain baseline data on cobalt-based Fischer-Tropsch synthesis.

Cobalt catalysts promoted with ruthenium or rhenium are reported to exhibit higher activity and better stability for Fischer-Tropsch synthesis. However, even with the same loading of promoters, catalysts prepared by different methods may exhibit performance that is quite different. Previously, promoted catalysts were prepared by multiple incipient wetness because of

the limited solubility in the small amount of water that can be utilized by this method and usually without calcination between the impregnation steps. The interaction between the cobalt and the promoter should have a significant impact upon catalyst performance. In this work, however, the catalysts were prepared by the incipient wetness technique with calcination after each cobalt impregnation. The cobalt should therefore be immobilized and the promoter effects for decreasing the reduction temperature, their impact on cobalt crystallite size and on the catalytic performance should be maximized. The following describes results of the preparation of two series of catalysts and the catalytic performance of one of the two series of catalysts is described in Task 9.

Preparation of Co-Re-Al_2O_3 catalysts

Three rhenium promoted cobalt catalysts were prepared. These preparations utilized a procedure that includes three cobalt impregnations followed by one rhenium impregnation; calcination steps were included between each impregnation step (calcination at 400ºC). Condea Vista B alumina, with a surface area of 200 m^2/g and pore volume of 0.4 cm^3/g, was used as the support. The cobalt loading for all three catalysts is 15 wt.% and rhenium loadings of 0.2, 0.5 and 1.0 wt.%, respectively, were used.

Three ruthenium promoted catalysts were prepared by the same method as described above for the Re-Co-Al_2O_3 catalysts. The cobalt loading again is 15 wt.% and the rhenium loadings are 0.2, 0.5 and 1.0 wt.%, respectively.

These catalysts will be characterized before and after utilization for Fischer-Tropsch synthesis performance (see Task 9 for performance results with the rhenium series catalysts).

Task 8. Cobalt Catalyst Testing for Activity and Kinetic Rate Correlations

The objective of this task is to conduct initial screening of the cobalt catalysts prepared in Task 7 to select three baseline catalysts that will then be used to generate a data base on the performance of cobalt-based Fischer-Tropsch catalysts in slurry reactors.

A. Effect of Water on the Fischer-Tropsch Catalytic Properties of Ruthenium Promoted Co/TiO_2 Catalyst

Introduction

Fischer-Tropsch synthesis produces hydrocarbons and water. The amount of water produced depends on the synthesis gas conversion, reactor system and catalyst used. The effect of water on the iron Fischer-Tropsch catalysts has widely been investigated. It is well known that water may reoxidize iron during synhesis [1]. Less information is available for the effect of water on the cobalt catalysts. Hilmen et al. [2] recently studied the effect of water on Co/Al_2O_3 and $CoRe/Al_2O_3$ catalysts by adding water to the synthesis gas feed and by model studies exposing the catalysts to various H_2O/H_2 ratios. It was found that the catalysts deactivated when water was added during Fischer-Tropsch synthesis and the catalysts oxidized in H_2O/H_2 mixtures with a ratio much lower than expected for oxidation of bulk cobalt. For silica supported cobalt catalysts, the addition of water to synthesis gas feed has been shown to decrease the CO conversion [3]. Schulz et al [4] found no deactivation of a $CO/Ru/ZrO_2$/Aerosil and $Co/MgO/ThO_2$/Aerosil catalysts when water was added to the feed. Schulz et al. [5] has even reported increased activity. Kim et al. [6, 7] also reported increased activity for Re promoted, non-promoted Co/TiO_2 and unsupported cobalt catalysts as a result of addition of water during the Fischer-Tropsch synthesis. It has been explained that water possibly destroys the strong metal-support interaction (SMSI) effect in titania supported catalysts. In this study, the effect of

water addition on the Fischer-Tropsch catalytic properties of a ruthenium promoted Co/TiO_2 catalyst was investigated. The incipient wetness technique was applied to prepare the catalyst and catalytic properties were evaluated in a continuous stirred tank reactor (CSTR) by using varying space velocities.

Experimental

The catalyst used was $Ru(0.2\ wt\%)Co(10wt\%)/TiO_2$ prepared in our laboratory, and was found to have good Fischer-Tropsch activity and stability. The catalyst activation was conducted first *ex-situ* and then *in-situ*, according to the following procedure. The catalyst (about 15 g) was put in a fixed bed reactor and pure hydrogen was introduced at a flow rate of 60 NLh^{-1} (298 K, 0.1 MPa); the reactor temperature was increased from room temperature to 373 K at a rate of 120 Kh^{-1}, then increased to 573 K at a rate of 60 Kh^{-1} and kept 573 K for 16 h. The catalyst was transferred under the protection of helium to the CSTR where it was mixed with 300 g of melted poly-wax (P.W. 3000). The catalyst was then reduced *in-situ* in the CSTR; the hydrogen was introduced to reactor at atmospheric pressure with a flow rate of 30 NLh^{-1} (298 K, 0.1 MPa). The reactor temperature was increased to 553 K at a rate 120 K h^{-1} and maintained at this activation condition for 24 h.

After the activation period, the reactor temperature was decreased to 483 K and synthesis gas ($2H_2/CO$) was introduced to increase the reactor pressure to 2.35 MPa. The reactor temperature was then increased to 503 K at a rate of 10 Kh^{-1}. During the entire run the reactor temperature was 503 K, the pressure was 2.35 MPa, and the stirring speed was maintained at 750 rpm.

The space velocity of the synthesis gas varied from 1 to 8 NL $g^{-1}cat.h^{-1}$. Argon was added to the feed gas and the composition was set to $2H_2/1CO/0.5Ar$. In order to investigate the effect

of water on the catalytic properties of the catalyst, argon was substituted by same amount of water at different space velocity. The conversion of carbon monoxide and hydrogen and the formation of products were measured after a period of 24 h at each condition.

Results and Discussion

Four runs have been done for the effect of water on the catalytic properties of the $RuCo/TiO_2$ Fischer-Tropsch catalyst using different space velocity procedures. The results for synthesis gas conversion are exhibited in Figures 1 and 2. For the first run, we started run with a space velocity of 2 $NLg^{-1}cat.h^{-1}$, then gradually increased the space velocity to 5, 7 and 8 $Nlg^{-1}cat.h^{-1}$, respectively, to obtain the activity and selectivity data at different space velocities. After running at 8 $NLg^{-1}cat.h^{-1}$, the catalyst was treated with pure CO for 24 hours. It was found that CO treatment resulted in a decreased Fischer-Tropsch activity. The catalyst was regenerated by pure H_2 and the space velocity was then changed back to 1 $NLgcat.^{-1}h^{-1}$. The synthesis gas conversion was found to be almost the same as that obtained at space velocity of 2 $NLg^{-1}cat.h^{-1}$ before CO treatment. This indicates that the activity of the catalyst was not be recovered by the H_2 regeneration at 230°C. For the second run, we started the run with a low space velocity and obtained almost 100% CO conversion. However, when we changed space velocity to 2 $NLg^{-1}cat.h^{-1}$, the synthesis gas conversion decreased to about 50%, indicating that the reaction at high conversion level resulted in a deactivation of the catalyst. The results for the third run are strange, synthesis gas conversion decreased with decreasing space velocity, indicating that the catalyst deactivated very quickly. This appears to be due to a problem in the catalyst reduction procedure for that particular run. For the fourth run (Figure 2), we started the run with a space velocity of 7 $NLg^{-1}cat.h^{-1}$, then decreased the space velocity to 4, 2 and 1 $NLg^{-1}cat.h^{-1}$,

respectively. The results were very similar to those obtained for first run except the data at space velocity of 1 $NLg^{-1}cat.h^{-1}$, which is much high than that of first and lower than second run.

During the fourth run, the water deactivation tests were made at synthesis gas space velocity of 2 $NLgcat.^{-1}h^{-1}$ by changing water flow back to same argon flow after feeding water for an extended period. The synthesis gas conversion was found to remain the same as that obtained before the water addition. This indicated that the water addition did not cause a permanent deactivation of the catalyst.

From Figure 2, we can find that at low conversion levels (high space velocities; greater than 4 $NLg^{-1}cat.h^{-1}$), the addition of water to the feed did not have a significant effect on synthesis gas conversion. However, at high conversion levels (low space velocities), the addition of water resulted in a decrease in synthesis gas conversion. The higher the conversion, the more severe the water effect is. This indicates that the Fischer-Tropsch reaction rate is dependent on the partial pressure of water for the ruthenium promoted Co/TiO_2 catalyst and a P_{H_2O} term existed in the kinetic equation. The Fischer-Tropsch synthesis kinetics of cobalt catalysts have been investigated by some researchers. However, for all the kinetic equations P_{H_2O} term has not been included. A kinetic investigation for cobalt catalyst is being done in our laboratory.

The effect of water on the hydrocarbon production rate of catalyst is shown in Figure 3. The hydrocarbon rate increased with increasing space velocity for no water and adding water reaction systems. At high space velocities, the addition of water did not influence hydrocarbon rate. At low space velocities, the addition of water resulted in a decrease in the hydrocarbon rate.

Figure 4 shows methane selectivity vs space velocity. For no water addition, the methane selectivity increased slightly with increasing space velocity. Methane selectivity did change with the addition of water.

Figure 5 shows CO_2 selectivity as a function of reciprocal flow rate. CO_2 selectivity increased almost linearly with decreasing space velocity (increasing conversion) with and without water addition. The addition of water increased the CO_2 formation about two times that of no water addition. This indicates that water also increased the water gas shift reaction.

References

1. M.E. Dry, Catal. Lett. 7 (1990) 204.
2. A.M. Hilmen, D. Schanke, K.F. Hanssen, A. Holmen, Appl. Catal. 186 (1999) 169.
3. J.K. Minderhoud, M.F.M. Post, S.T. Sie, Eur. Appl. Patent No. 83201557.2 (1988), to Shell Int. Res.
4. H. Schulz, M. Claeys, S. Harms, Stud. Surf. Sci. Catal. 107 (1997) 193.
5. H. Schulz, E. van Steen, M. Claeys, Stud. Surf. Sci. Catal. 81 (1994) 455.
6. J.C. Kim, U.S. patent no. 5227407 (1993), to Exxon Res. Eng. Co.
7. J.C. Kim, Eur Appl. Patent no. 89304092.3 (1994), to Exxon Res. Eng. Co.

Fig. 1. Effect of water on the synthesis gas conversion of $RuCo/TiO_2$ F-T catalyst

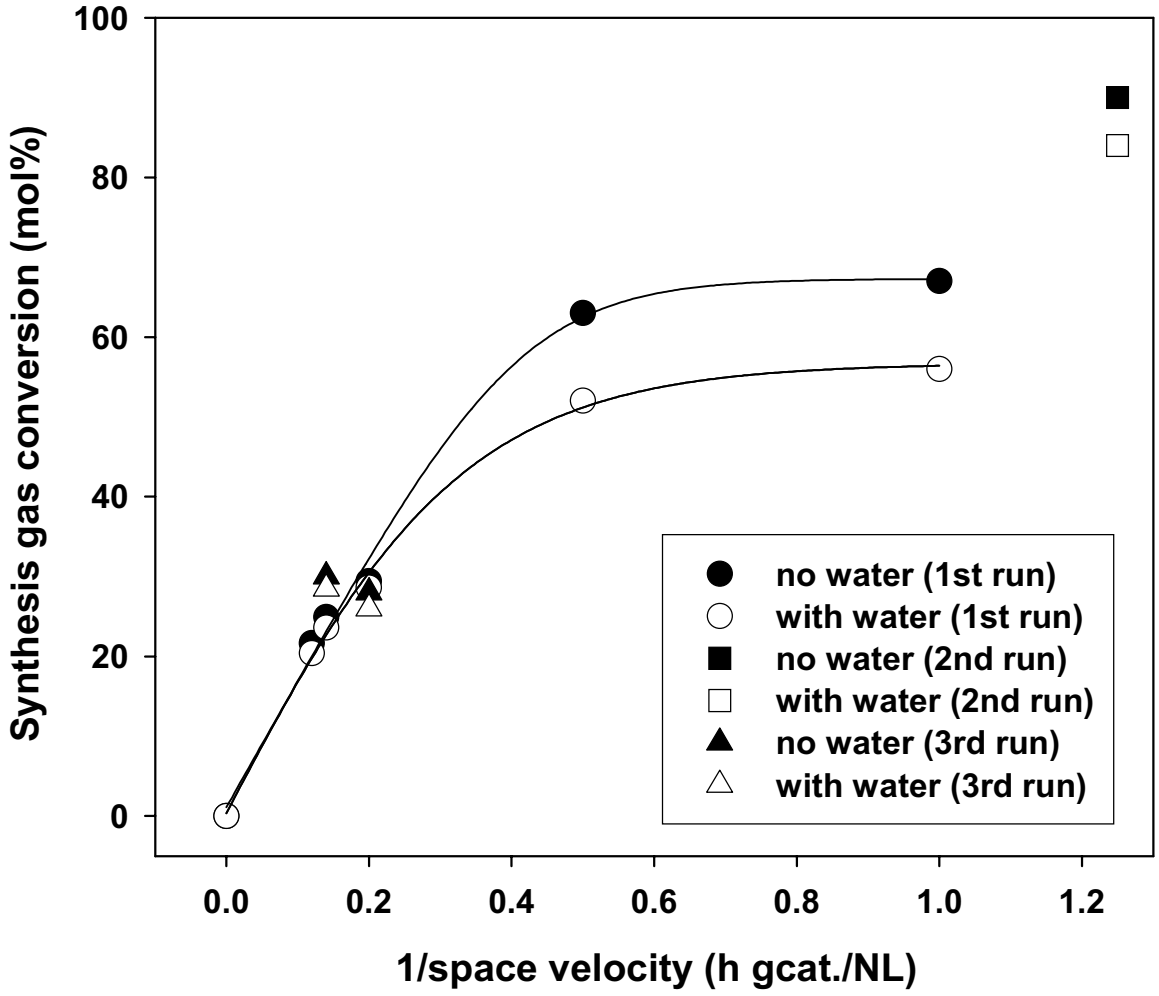

Fig. 2. Effect of water on synthesis gas conversion (fourth run)

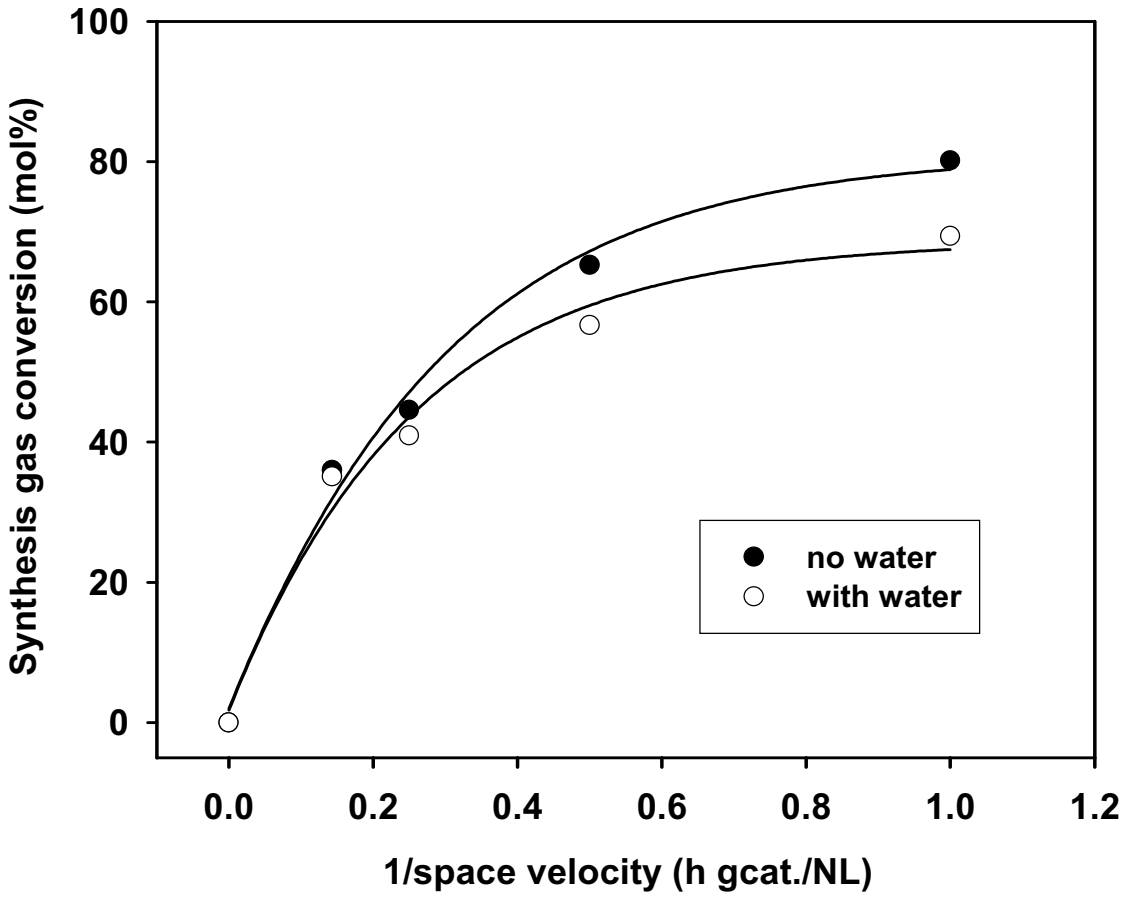

Fig. 3. Effect of water on hydrocarbon production rate

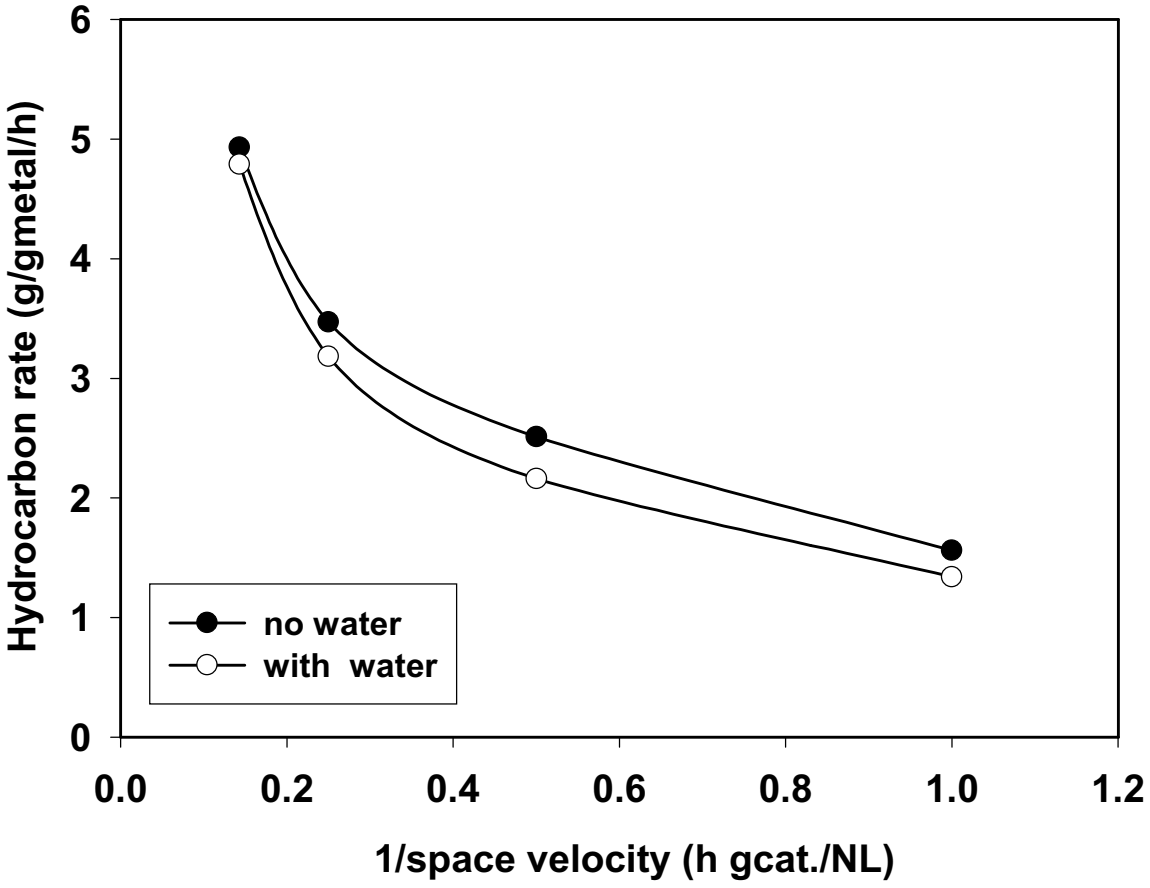

Fig. 4. Effect of water on methane selectivity

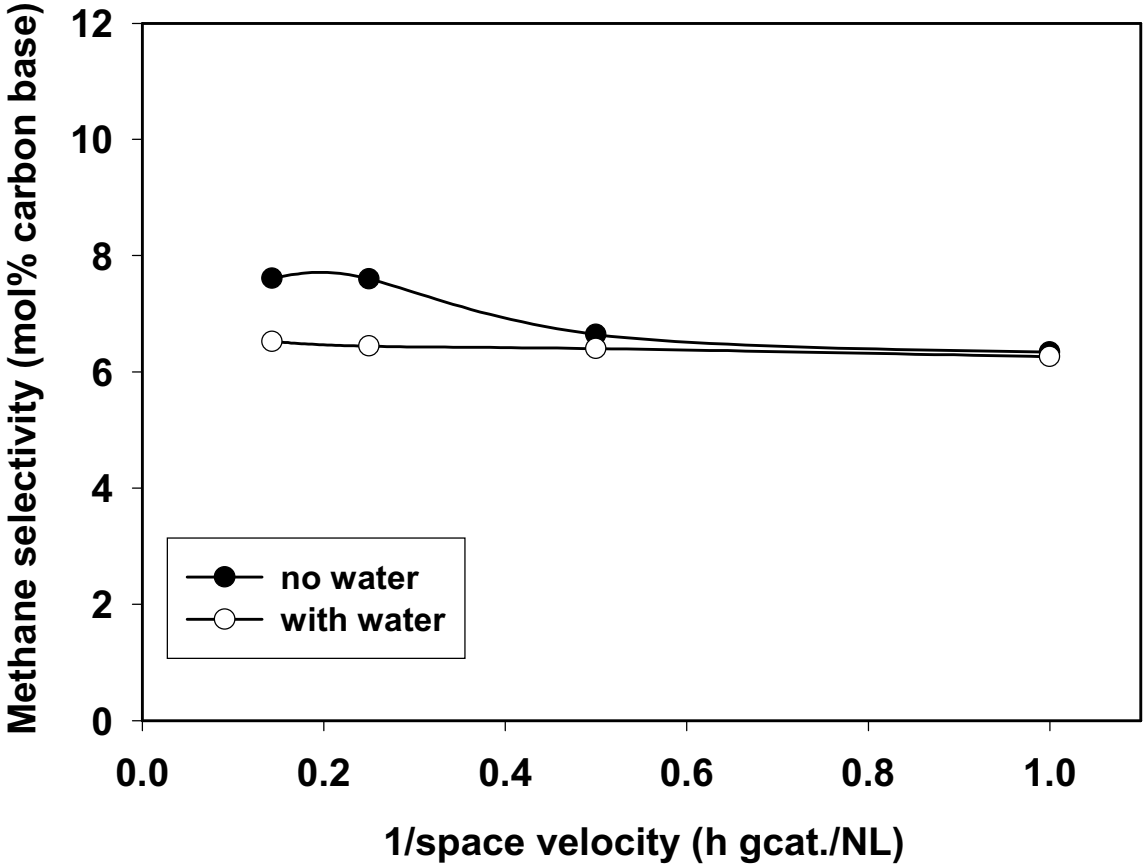

Fig. 5. Effect of water on CO_2 selectivity

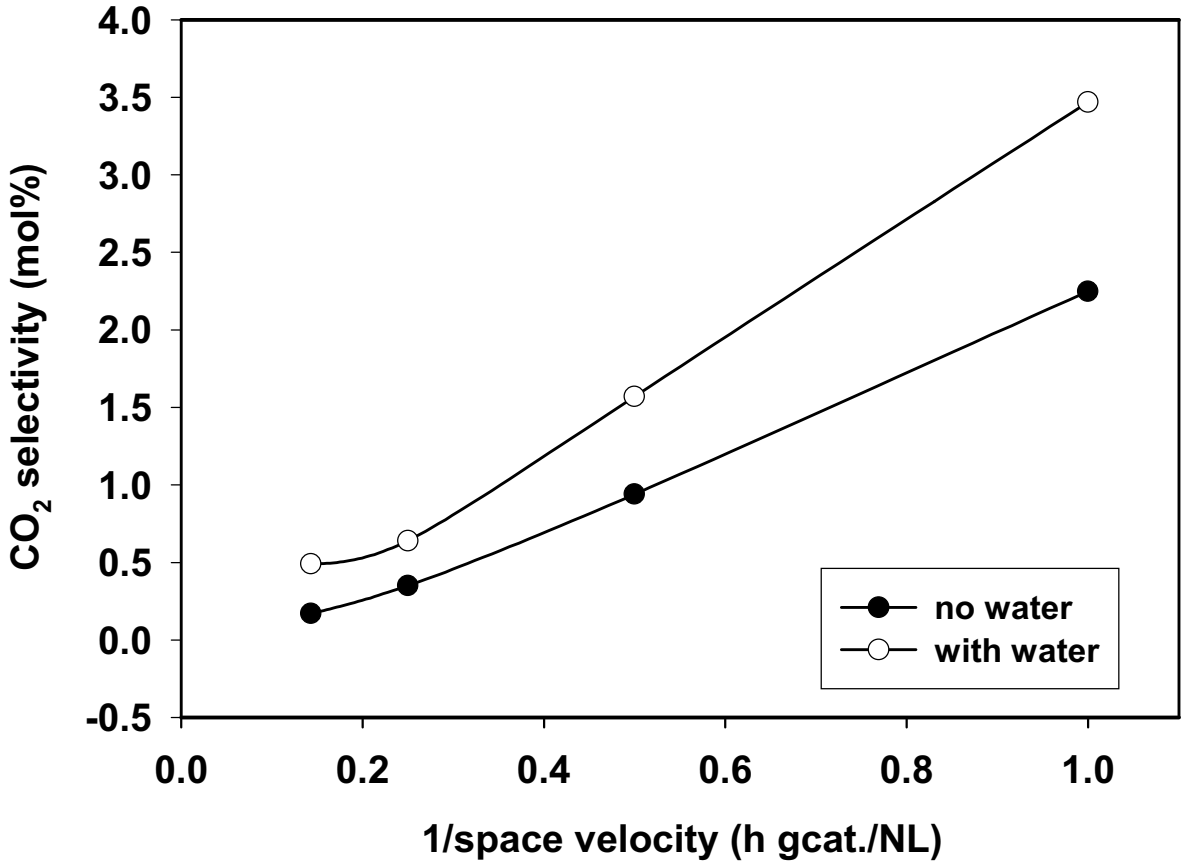

B. Activity of Cobalt Catalysts

The CO conversion is directly related to the reciprocal of the space velocity for the 0.2 and 1.0% Re containing Co-Al_2O_3 catalysts (Figures 1 and 2) for the range of zero to about 50% CO conversion. The data in Figures 1 and 2 are collected after the conversion has declined rapidly and is in the portion of the activity curve that represents a slow decline in activity region. This observation was reported during the last quarter for the Pt-Co-Al_2O_3 catalyst (Figure 3); however, for the highest CO conversion level there is deviation from linearity. This is presumably due to the presence of a high partial pressure of water relative to that of unconverted CO (and/or H_2). Based on the slope of the line for the 0.2 wt.% Re catalyst, the productivity is 0.13 g hydrocarbon/g cat./hr and for the 1.0 wt.% Re catalyst the productivity is 0.65 g hydrocarbon/g cat./hr. The productivity of the 1.0 wt.% Pt catalyst is essentially the same as has been found for the 1.0 wt.% Re catalyst. These productivities are similar, or exceed, to those reported by Sasol workers for their active cobalt catalysts (1).

For the 0.2 wt.% Re catalyst, CO conversion increases slowly as the total pressure, with $H_2/CO = 2.0$, as the pressure is increased from 275 (18.7 atm; 1.9 MPa) to 450 psig (30.6 atm; 3.1 MPa) (Figure 4). Thus, these catalysts are approaching the plateau where the conversion is nearly independent of the total pressure provided $H_2/CO = 2.0$.

The methane selectivity for the 0.2 wt.% Re catalyst is nearly 15 molar% of the total hydrocarbons produced (Figure 5). The amount of methane produced is essentially constant over the pressure range used (275 to 450 psig).

Additional analysis of the reaction products are underway and will be reported in the next quarterly report.

References

1. R. L. Espinoza, J. L. Visage, P. J. van Berge and F. H. Holder, U.S. 5,733,839, March 31, 1998.

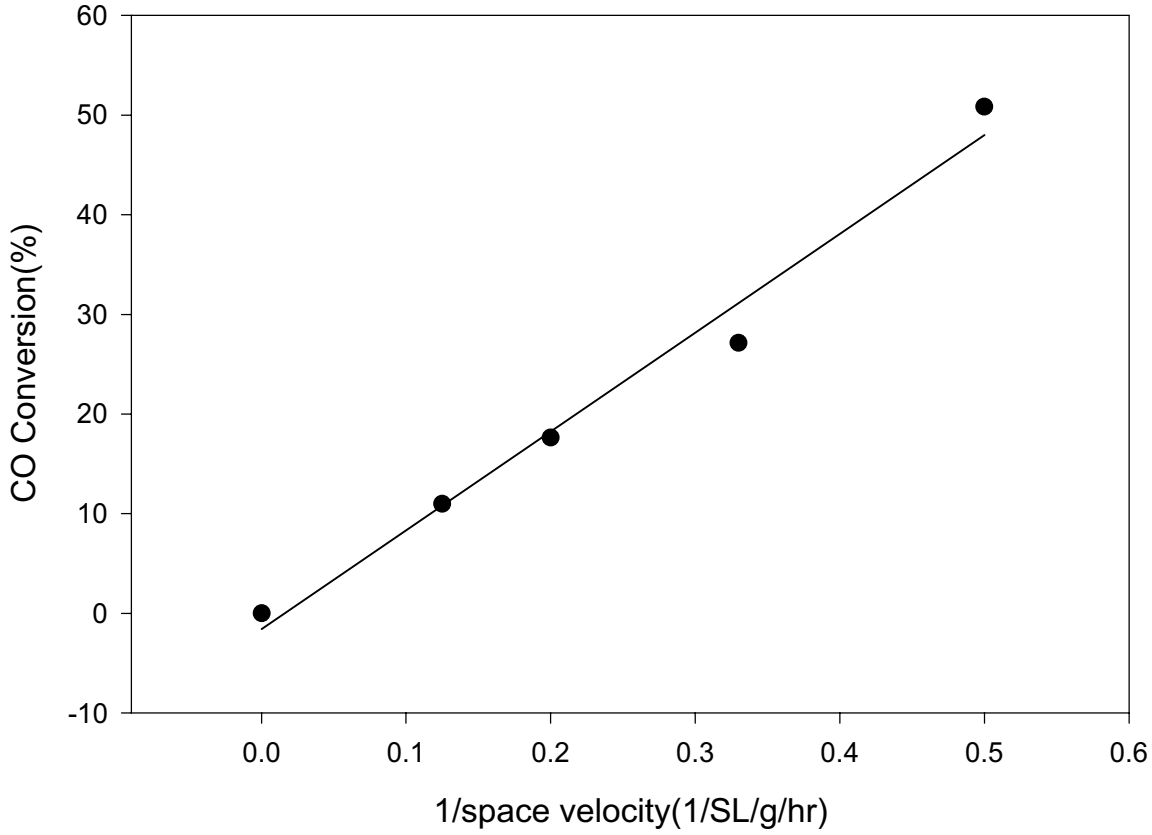

Fig 1. CO conversion as a function of space time on 15%Co-1.0%Re/Al_2O_3

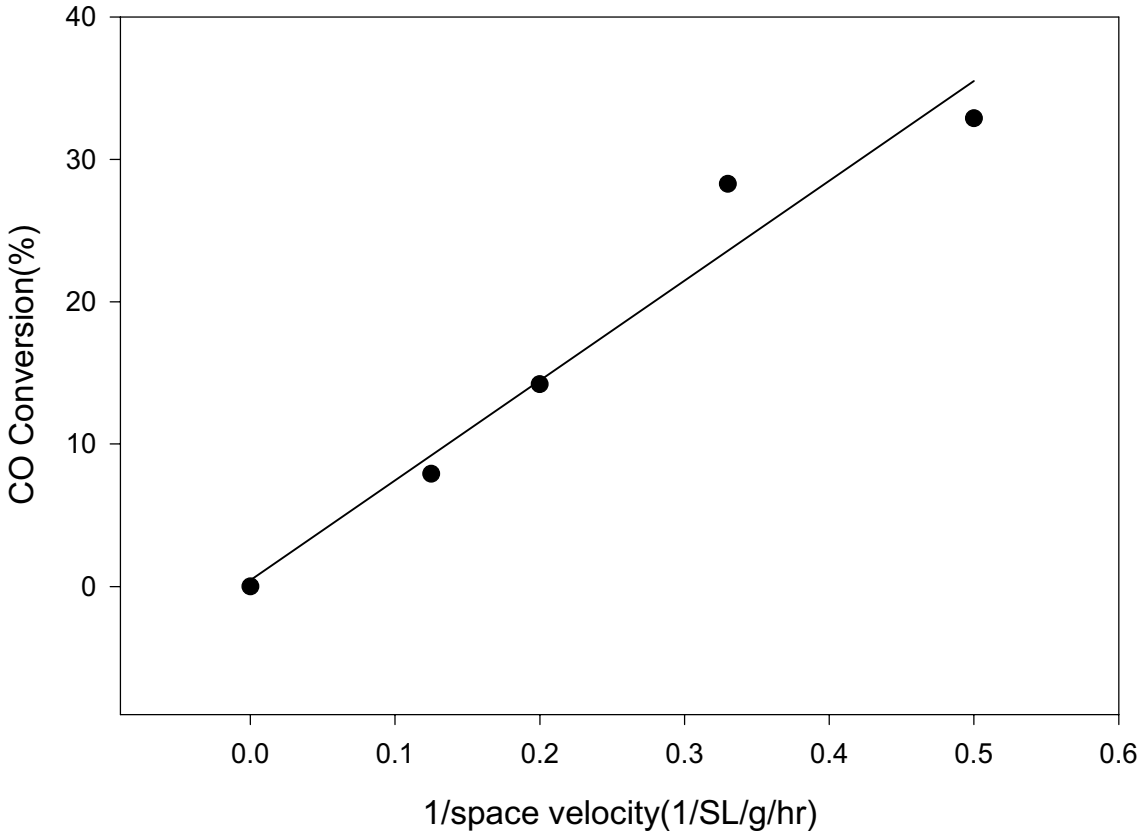

Fig 2. CO conversion as a function of space time for 15%Co-0.2%Re/Al_2O_3

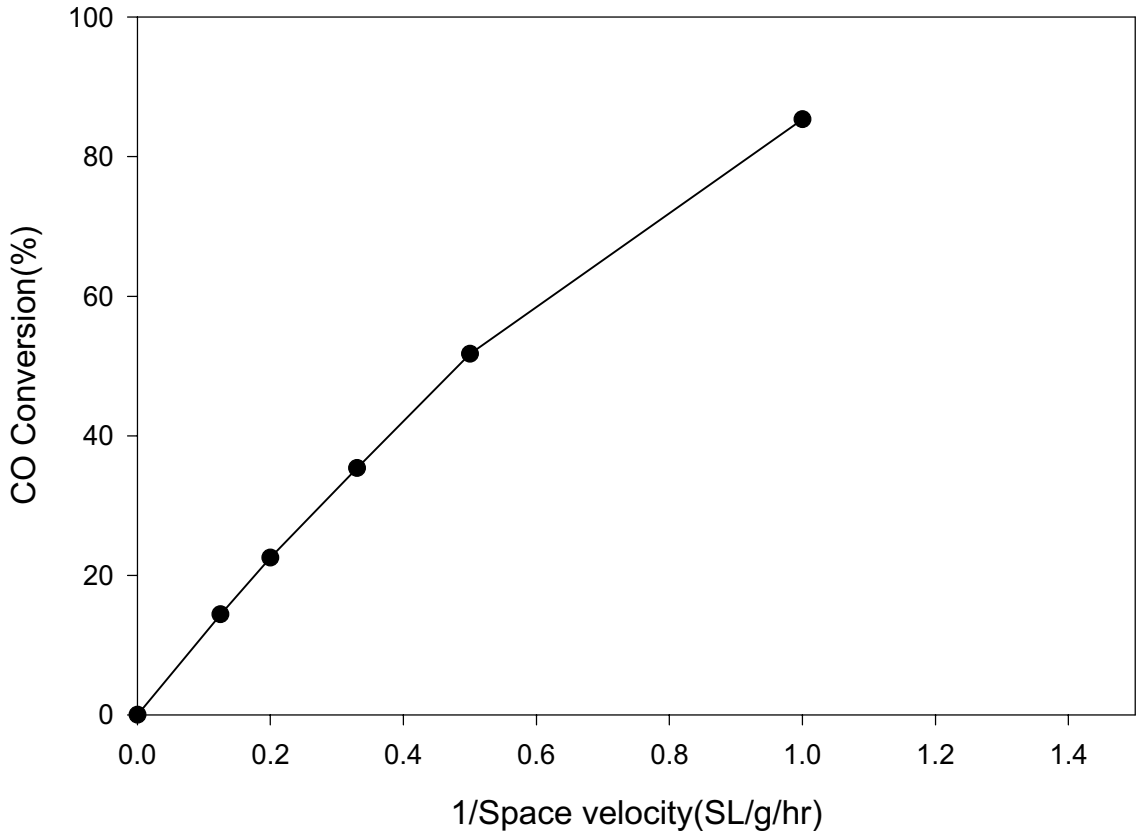

Fig 3. CO conversion as a function of space time on 15%Co-0.5%Pt/Al_2O_3

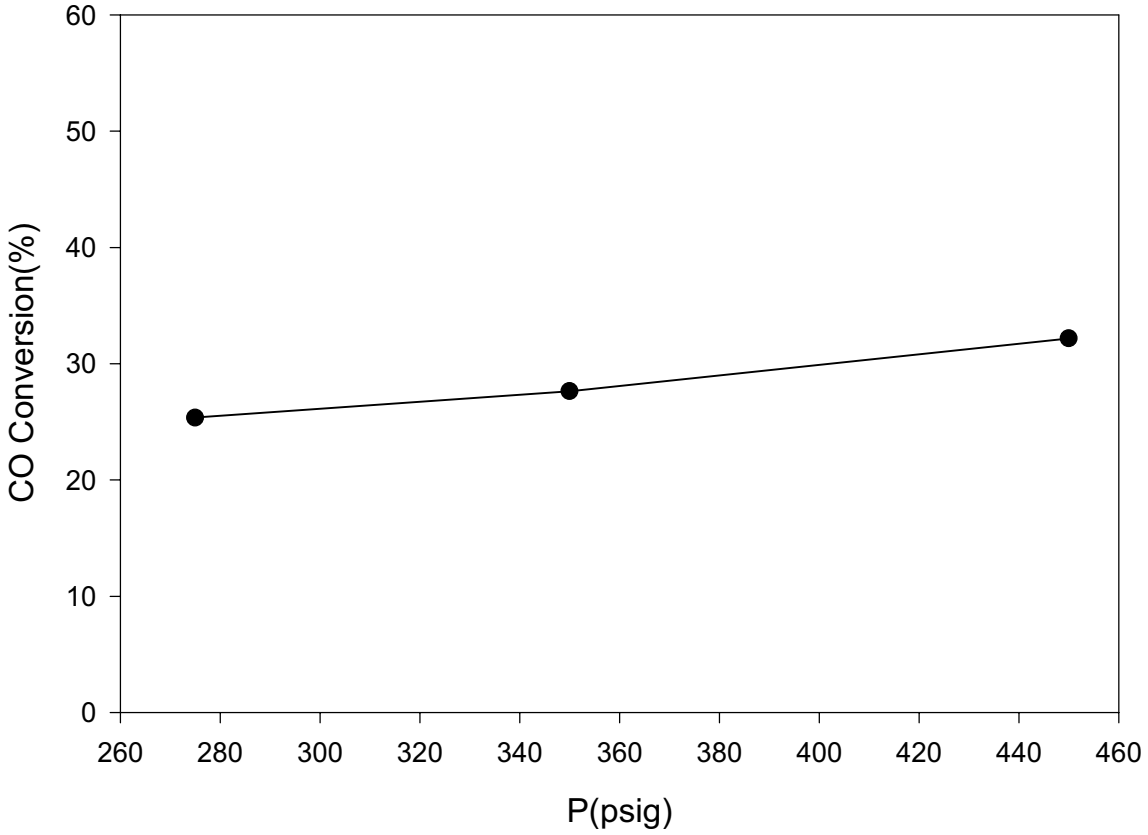

Fig 4. The effect of pressure to CO conversion on 15%Co-0.2%Re/Al_2O_3

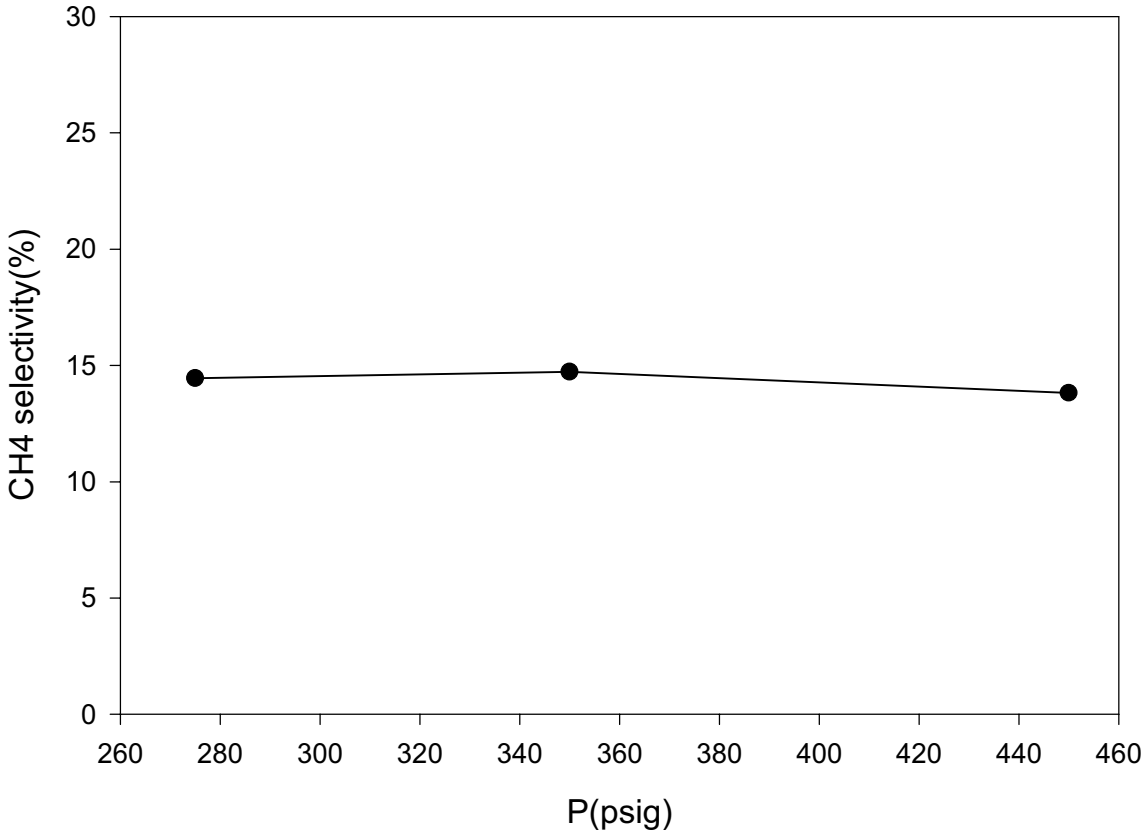

Fig 5. Methane selectivity as a function of pressure on 15%Co-0.2Re/Al_2O_3 catalyst